UNCLASSIFIED

S-532

MICROWAVE FERROELECTRICS

RAYTHEON

Report No. 10
Contract No. DA 36-039-sc-89126
Order No. 40750 - PM-61-93-93
Continuation of Contract No. DA 36-039-sc-87369

Sixth Quarterly Progress Report

16 December 1962 - 15 March 1963

U.S. Army Electronics Research and Development Laboratory

Fort Monmouth, New Jersey

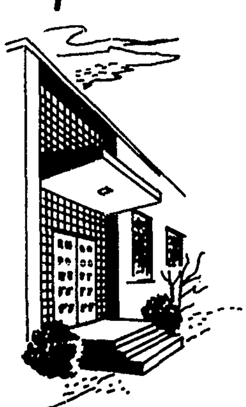

RESEARCH DIVISION
RAYTHEON COMPANY
WALTHAM 54, MASSACHUSETTS

S-532

MICROWAVE FERROELECTRICS

Report No. 10

Contract No. DA 36-039-sc-89126

Order No. 40750-PM-61-93-93

Sixth Quarterly Progress Report

16 December 1962 - 15 March 1963

Object

To conduct research and development investigations to develop nonlinear dielectric materials.

Prepared by

B. di Benedetto, M. Harris, P. B. Nutter

TABLE OF CONTENTS

1. PURPOSE 1

2. ABSTRACT 2

3. PUBLICATIONS AND CONFERENCES 3

3.1 Publications 3

3.2 Conferences 3

4. FACTUAL DATA 4

4.1 Dielectric Constant and Nonlinearity of Stannate Doped BST-50 Samples 4

4.1.1 S-band measurements of dielectric constant 4

4.1.2 S-band nonlinearity measurements at constant frequency 8

4.1.3 S-band nonlinearity measurements at constant temperature 12

4.2 Loss Tangents of Stannate Doped BST-50 Samples 16

4.3 Low Frequency Dielectric Constants and Nonlinearity of Stannate Doped BST-50 Samples 16

4.4 The Preparation and Microstructure of the Stannate Doped BST-50 Materials 19

4.5 Dielectric Constant and Loss Tangent of Hafnate Doped BST-50 Samples 21

4.6 Dielectric Constant and Loss Tangent of $Cd_2Nb_2O_7$ Ceramic.. 25

4.7 Measurement of Field-Dependent Loss and Nonlinearity in BST-50 25

4.7.1 Apparatus and procedure 25

4.7.2 Skin losses 33

4.7.3 Field dependent losses in BST-50 35

4.8 Time Stability of Dielectric Constant in BST-50 + 1% $SrSnO_3$-B1 37

TABLE OF CONTENTS (Cont' d)

5. CONCLUSIONS 38

5.1 The Stannate Doped BST-50 Materials 38

5.2 The Hafnate Doped BST-50 Materials 43

5.3. The $Cd_2Nb_2O_7$ Ceramic 43

5.4 The Field Dependent Losses and Nonlinearity in BST-50 43

5.5 The Time Dependance of Dielectric Constant in BST-50 45

6. PLANS FOR THE NEXT QUARTER 48

7. ACKNOWLEDGMENTS 49

8. IDENTIFICATION OF PERSONNEL 50

LIST OF FIGURES

Number	Title	Page
1	Curie Plot of Dielectric Constant vs Temperature for BST-50 + 1 % $SrSnO_3$-B2	5
2	Curie Plot of Dielectric Constant vs Temperature for BST-50 +1% $SrSnO_3$-C1	6
3	Curie Plot of Dielectric Constant vs Temperature for BST-50 +1% $SrSnO_3$-G1	7
4	Nonlinearity Plot for BST-50 + 1% $SrSnO_3$-B2	9
5	Nonlinearity Plot for BST-50 + 1% $SrSnO_3$-C1	10
6	Reduced Nonlinearities for Various BST-50 Dopings	13
7	Reduced Nonlinearity for BST-50 + 1% $SrSnO_3$-B1 Measured at Constant Temperature	14
8	Reduced Nonlinearity for BST-50 + 1% $SrSnO_3$-G2 Measured at Constant Temperature	15
9	Loss Tangent vs Temperature for BST-50 + 1% $SrSnO_3$ Samples	17
10	Dielectric Constant vs Temperature for BST-50 + 1% $SrSnO_3$ Samples	18
11	Reduced Nonlinearity for BST-50 + 1% $SrSnO_3$-B Near the Curie Temperature	20
12	Photomicrographs of Samples B, C, E	22
13	Photomicrographs of Samples F, G, H, I	23
14	Photomicrographs of Sample E	24
15	Curie Plot of Dielectric Constant vs Temperature for BST-50 + 1% $BaHfO_3$ and BST-50 + 2% $BaHfO_3$	26
16	Loss Tangent vs Temperature for BST-50 Doped with $BaHfO_3$	27
17	Curie Plot of Dielectric Constant vs Temperature for Ceramic $Cd_2Nb_2O_7$	28
18	Loss Tangent vs Temperature for Ceramic $Cd_2Nb_2O_7$	29
19	Apparatus for Measurement of Field Dependent Losses at X-band	31
20	Field Dependent Loss in BST-50	36
21	Time Dependence of Dielectric Constant with Steady Applied Fields	46

1. PURPOSE

It is the purpose of this work to develop and investigate those materials which exhibit the properties of low loss, low dielectric constant, and high nonlinearity that are required for applications at microwave frequencies.

2. ABSTRACT

Several batches of $Ba_{0.5}Sr_{0.5}TiO_3 + 1\% SrSnO_3$ ceramic have been prepared and those which have been measured all exhibit a slightly larger nonlinearity than pure $Ba_{0.5}Sr_{0.5}TiO_3$ material. One sample only shows a markedly larger nonlinearity which has been confirmed by repeated measurements and by using different measuring techniques. The reason for its superiority over supposedly identical materials has not been established. Losses in other doped materials have been measured. The field dependent loss in $Ba_{0.5}Sr_{0.5}TiO_3$ material has been measured and an upper limit set upon its value. The value of the field dependent loss is small compared with the intrinsic zero-field loss at X-band, at 150°C and for fields of 1.6×10^6 volts/metre.

3. PUBLICATIONS AND CONFERENCES

3.1 Publications

None.

3.2 Conferences

On March 18, 1963 there was a conference at Raytheon Research Division between Mr. J. Charlton and Mr. C. Heinzman of the Signal Corps and Dr. P. B. Nutter and Mr. M. Harris of Raytheon Company. The work of the contract was discussed.

4. FACTUAL DATA

4.1 Dielectric Constant and Nonlinearity of Stannate Doped BST-50 Samples

4.1.1 S-band measurements of dielectric constant

Previous reports have given the results of measurements on two samples of $Ba_{0.5}Sr_{0.5}TiO_3$ doped with one percent of $SrSnO_3$. The present report presents data on other samples of similar material and it becomes necessary to use some code to distinguish the various samples. The sample referred to in Section 4.4 of Report No. 7 of this series will be referred to retrospectively as sample A and that of Section 4.3 in Report No. 9 will be referred to as sample B. All current and future samples will be coded in alphabetic order as they are produced. Where more than one experimental piece is cut from each prepared batch the pieces will be distinguished as B1, B2, etc. All samples will have their constitution specified as BST-50 + 1% $SrSnO_3$ for brevity.

Dielectric constants for various stannate doped BST-50 materials were measured at S-band over the temperature range 220 – 320°K. The measurements were obtained by the usual technique of observing microwave cavity resonances at known frequencies in samples of known simple geometry.

The results are displayed in the form of a Curie plot $1/\epsilon$ vs T in Fig. 1, 2, and 3. Figure 1 gives the data for BST-50 + 1%$SrSnO_3$-B2 which is a second portion of the same material measured and reported previously.[1] Figures 2 and 3 give measurements on more recently prepared material. The data is summarized in Table 1.

---

[1] See Section 4.3, Report No. 9 of this series. The sample reported here has been subsequently coded as BST-50 + 1%$SrSnO_3$-B1.

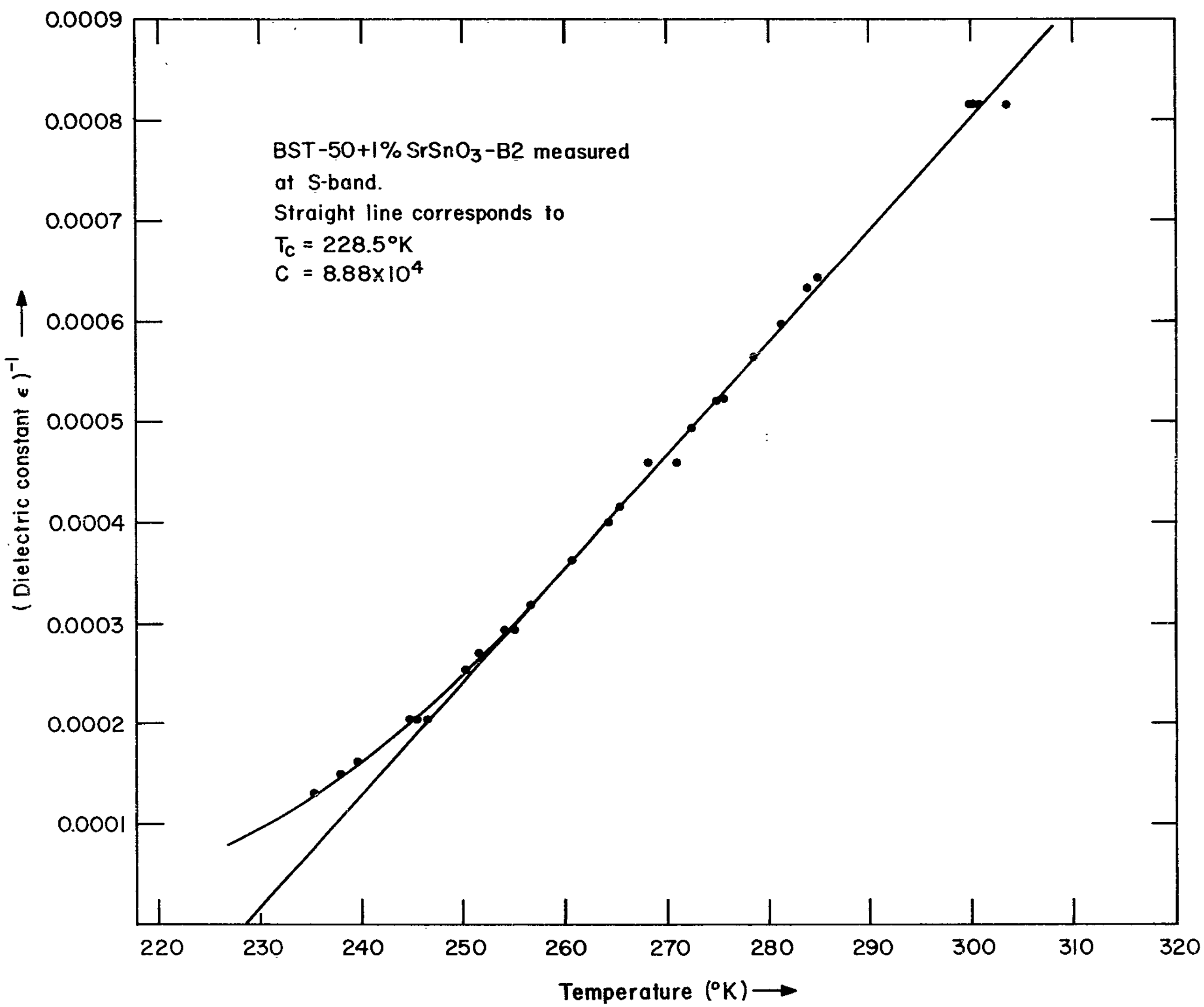

CURIE PLOT OF DIELECTRIC CONSTANT VS TEMPERATURE FOR BST-50+1% $SrSnO_3$-B2

FIGURE 1

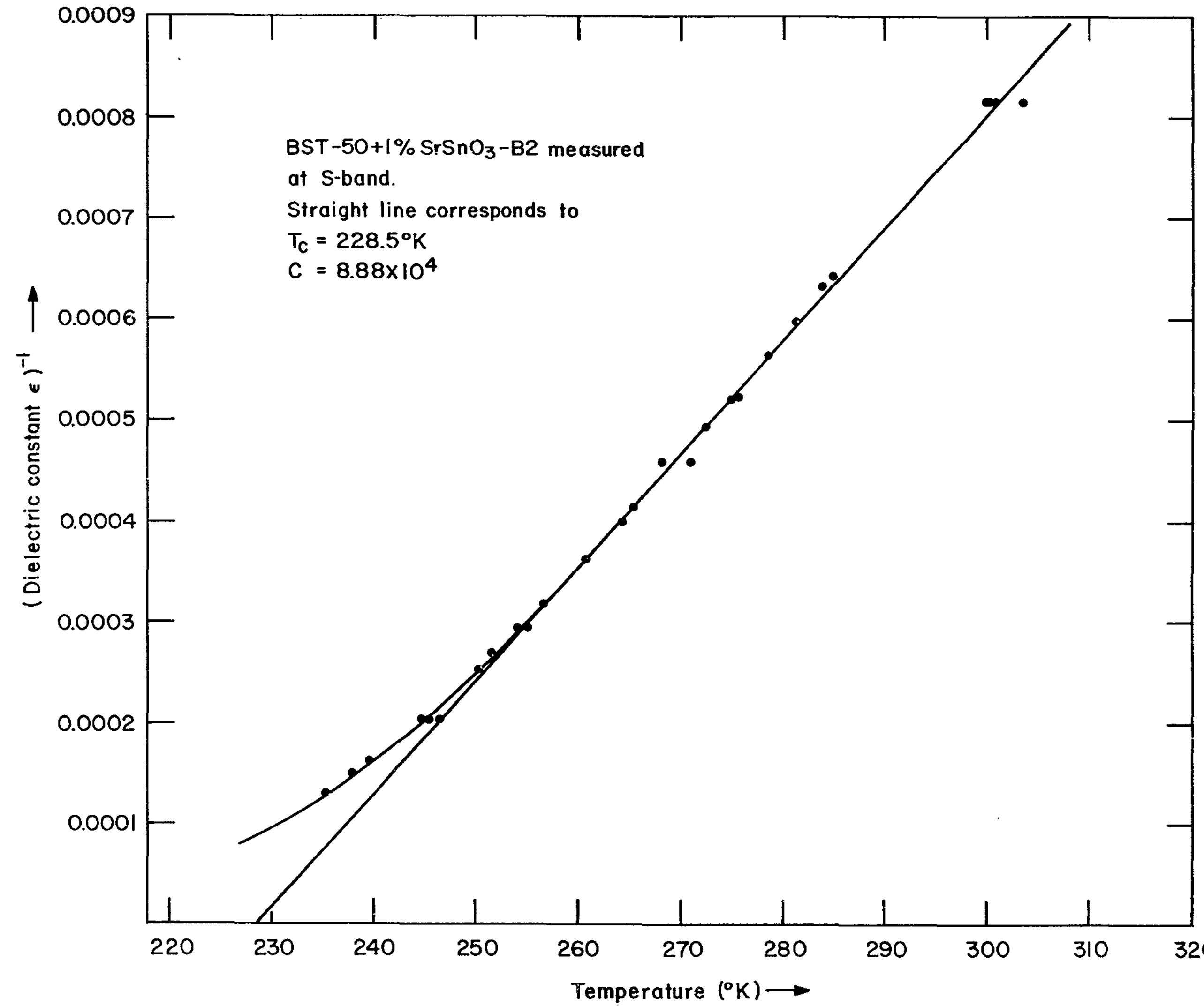

CURIE PLOT OF DIELECTRIC CONSTANT VS TEMPERATURE FOR BST-50+1% $SrSnO_3$-B2

FIGURE 1

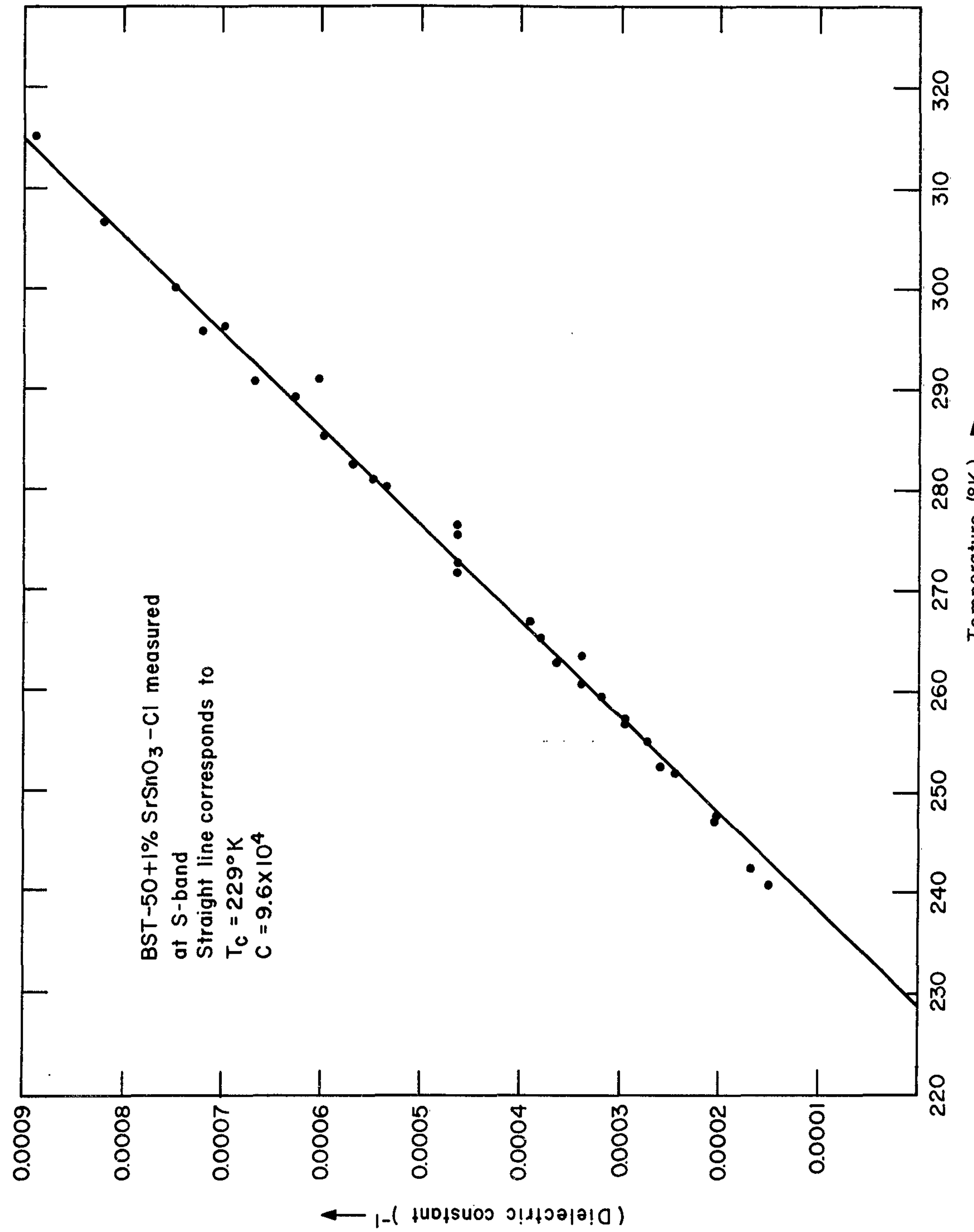

CURIE PLOT OF DIELECTRIC CONSTANT VS TEMPERATURE FOR BST-50+1% $SrSnO_3$-Cl

FIGURE 2

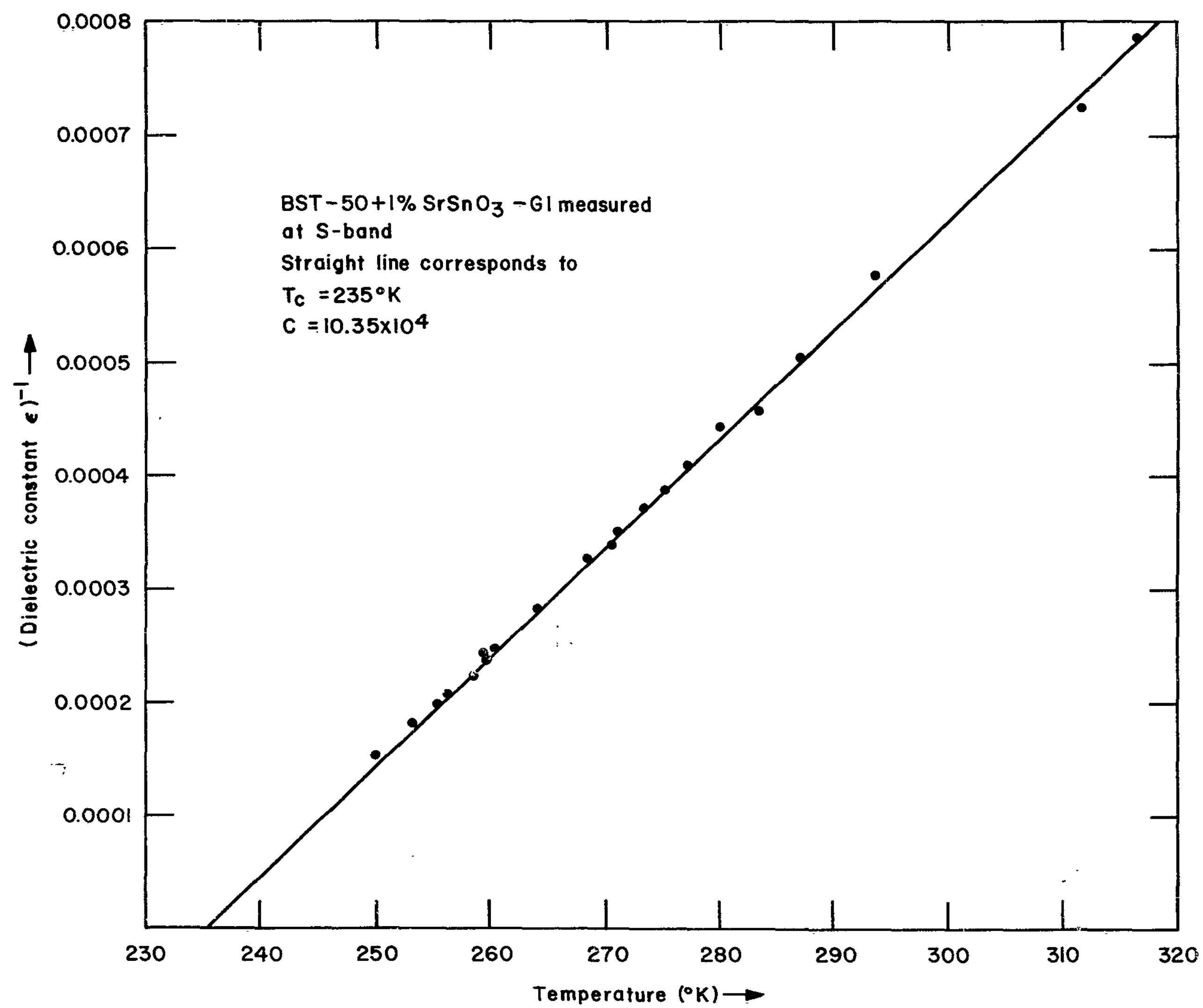

CURIE PLOT OF DIELECTRIC CONSTANT VS TEMPERATURE FOR BST-50+1% $SrSnO_3$ – G1

FIGURE 3

TABLE I

Material	Curie Constant	Curie Temp °K
BST-50 + 1% $SrSnO_3$-B2	8.88×10^4	228.5
BST-50 + 1% $SrSnO_3$-C1	9.60×10^4	229.0
BST-50 + 1% $SrSnO_3$-G1	10.35×10^4	235.0

4.1.2 S-band nonlinearity measurements at constant frequency

The dielectric nonlinearity was measured for samples B2 and C1 in the usual fashion, i.e., the microwave source is tuned until a resonance is observed in the sample at a chosen temperature. A uniform electric field of known magnitude is applied to the sample thereby lowering its dielectric constant and rendering the sample nonresonant at the fixed source frequency. The temperature of the sample is then lowered until the dielectric constant is restored to its original value at which point the original resonance is restored and can be observed. Under conditions where the expression for the field dependence of the dielectric constant

$$\epsilon(T, E) = \frac{\epsilon(T, O)}{1 + \frac{A}{C}\epsilon^3(T, O)E^2} \tag{1}$$

is valid, and so long as the Curie law is obeyed over the temperature range of the experiment, it can be shown that the temperature drop ΔT needed to restore resonance after application of a field E is given by:

$$\sqrt{\Delta T} = \epsilon\sqrt{A} \, . \, E \tag{2}$$

The data are presented in Fig. 4 and 5 as graphs of $(\Delta T)^{\frac{1}{2}}$ vs E for various starting temperatures in the range 5 - 40°C for the materials B2 and C1 respectively. Both graphs show departures from the straight line expressed by Eq. 2 but use of the slope of the fairly straight portions below $E = 10^6$ volts/meter enables us to extract reasonable values for the nonlinearity coefficient A.

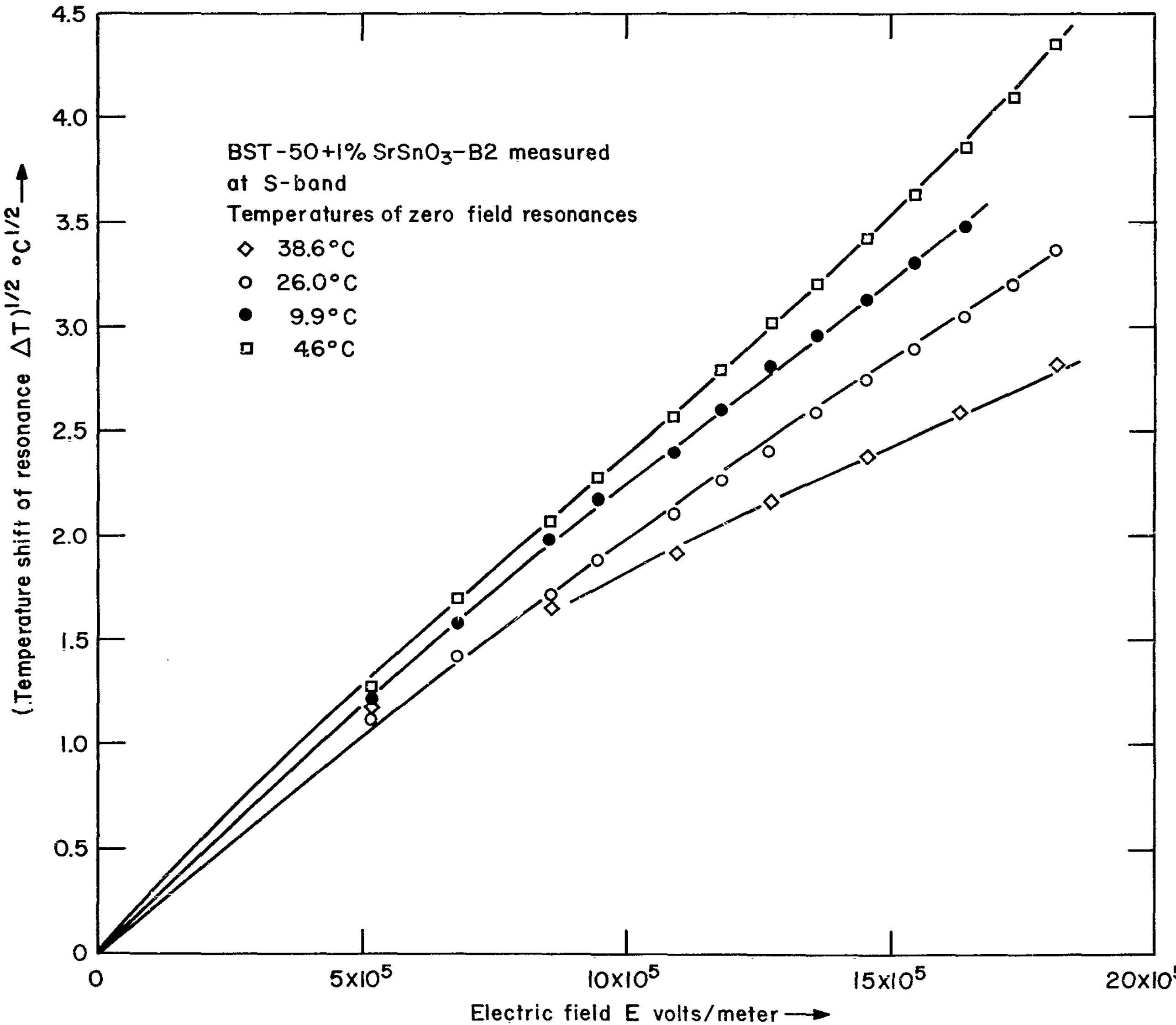

NON-LINEARITY PLOT FOR BST-50+1% $SrSnO_3$ -B2

FIGURE 4

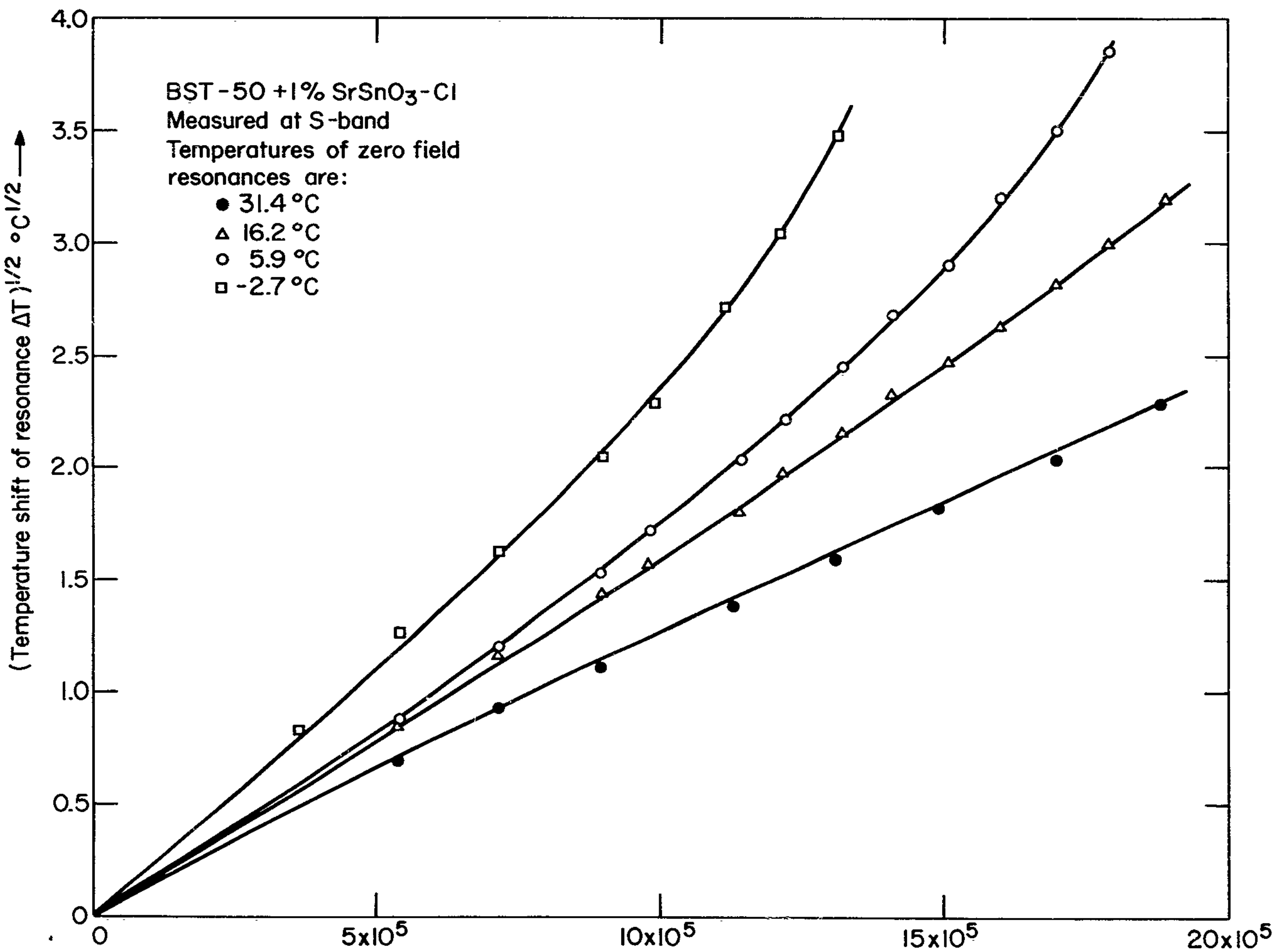

NONLINEARITY PLOT FOR BST-50 +1% $SrSnO_3$ - Cl

FIGURE 5

The results of these measurements are summarized in Table II.

TABLE II

Material	Temp (°C)	$A°K \cdot m^2/V^2$
BST-50 + 1% $SrSnO_3$-B2	38.6	2.82×10^{-18}
	26.0	2.45×10^{-18}
	9.9	1.88×10^{-18}
	4.6	1.71×10^{-18}
BST-50 + 1% $SrSnO_3$-C1	31.6	1.00×10^{-18}
	16.2	0.99×10^{-18}
	5.9	0.76×10^{-18}
	-2.7	0.96×10^{-18}

Comparison of materials in respect of their nonlinearity is facilitated if the experimental data is presented in a different way. We introduce the concept of a "reduced nonlinearity at field E" and define it as

$$\eta(E, T) = \frac{\epsilon(T, O) - \epsilon(T, E)}{\epsilon(T, E)} \quad . \tag{3}$$

Manipulation of Eq. (1) shows that

$$\eta(E, T) = \frac{A}{C} \epsilon^3(T, O) E^2 \quad . \tag{4}$$

Using Eq. (2) and the Curie law for the dielectric constant $\epsilon(T, O)$ this transforms again into the expression

$$\eta(E, T) = \frac{\Delta T}{T - T_c} \quad . \tag{5}$$

Figure 6 plots $\eta(10^6, T)$ vs $(T-T_c)$ for materials B1,[2] B2, C1 and for an undoped sample of BST-50 ceramic.[3]

4.1.3 S-band nonlinearity measurements at constant temperature

Under conditions where the validity of Eq. (1) is in question or where there are marked divergences from the Curie law it is advantageous to measure the field dependence of the dielectric constant directly and at constant temperature. This may be done by measuring the resonant frequency of the dielectric cavity resonator both with and without an applied field. The equipment required to perform this measurement is a simplification of a previously reported setup[4] and the technique has been used before.[5] The simplifications referred to are: first, the omission of the calibrated precision step attenuator; and second, the substitution of a cavity wavemeter for the more sophisticated frequency measuring equipment. Both these were required to obtain exact measurements of peak widths in the original setup and this is not a feature of the current measurements.

The data are conveniently obtained and presented in the form of a reduced nonlinearity $\eta(E,T)$ as defined in Eq. (3). If resonances are observed at f_E and f_o for the same mode of excitation of the sample with and without field E it follows that

$$\eta(E,T) = \frac{f_E^2 - f_o^2}{f_o^2} \quad . \tag{6}$$

Figures 7 and 8 plot η vs E^2 at various temperatures from 20 - 40°C for the stannate doped BST-50 materials B1 and G2.

---

[2] Data from the original of Section 4.3 Report No. 9 of this series.

[3] Data from the original of Section 4.4 Report No. 9 of this series.

[4] See Fig. 4, Report No. 8 of this series.

[5] See Section 4.4, Report No. 8 of this series.

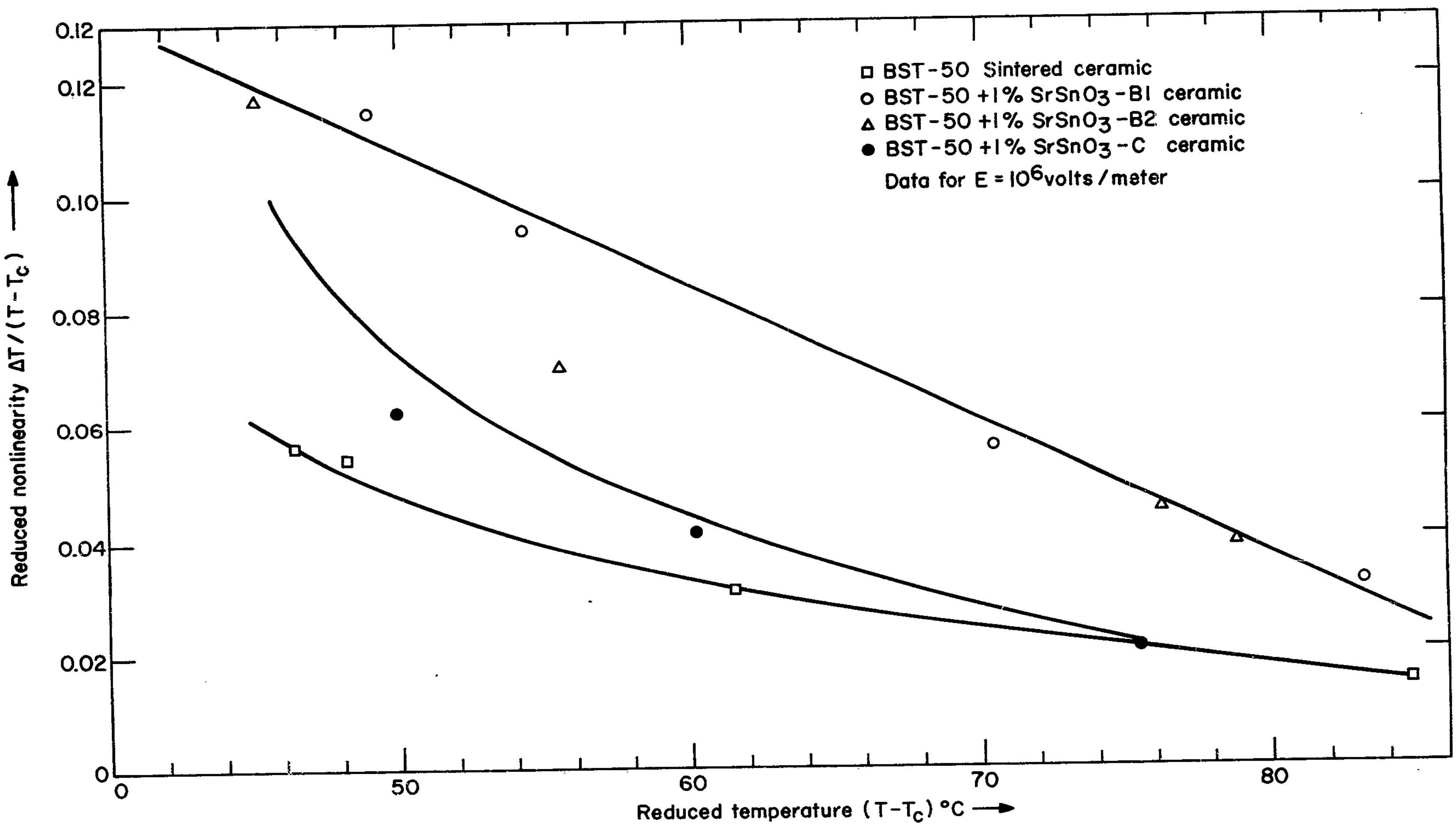

REDUCED NONLINEARITIES FOR VARIOUS BST-50 DOPINGS

FIGURE 6

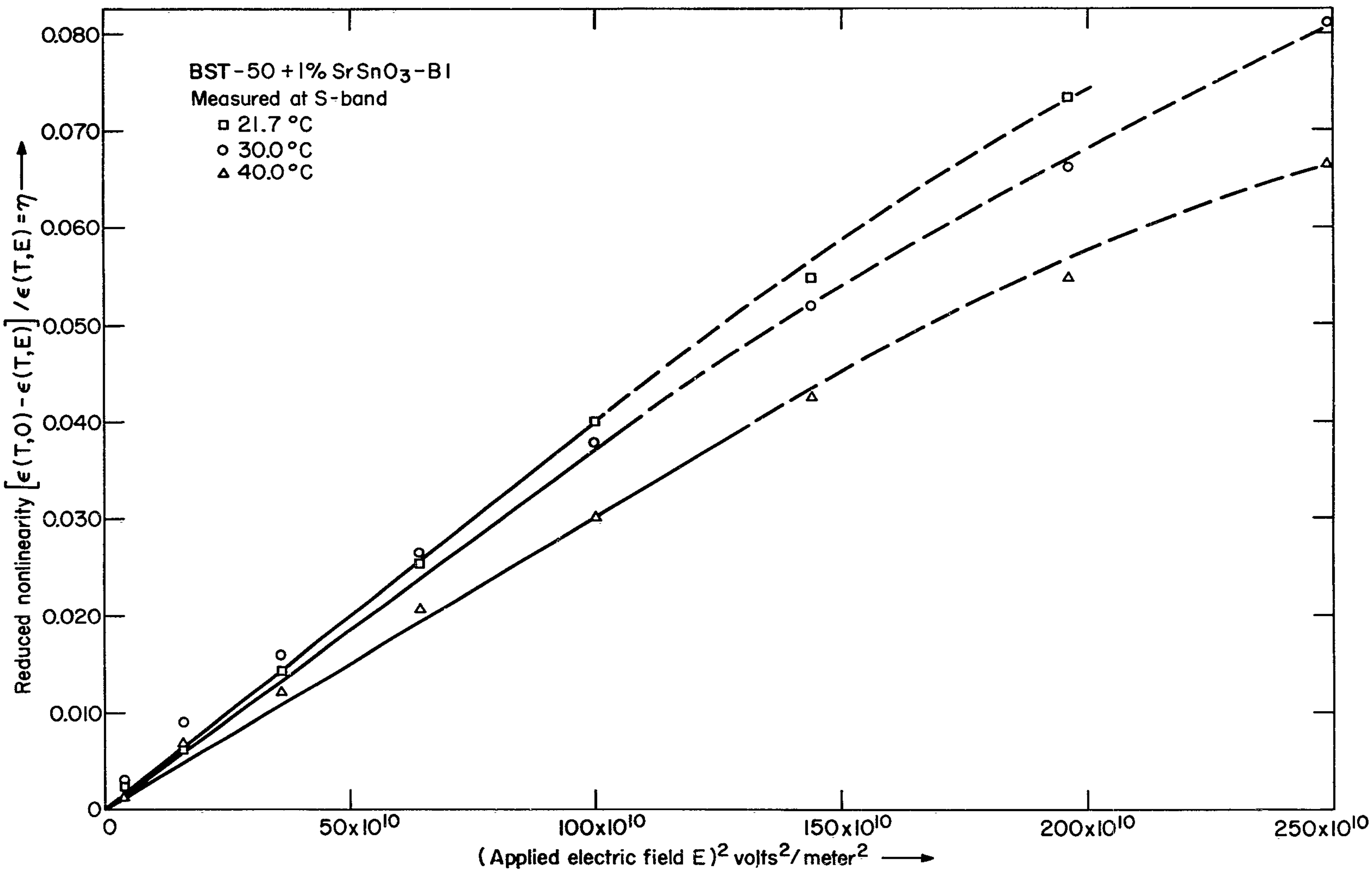

REDUCED NONLINEARITY FOR BST-50 + 1% $SrSnO_3$-B1 MEASURED AT CONSTANT TEMPERATURE

FIGURE 7

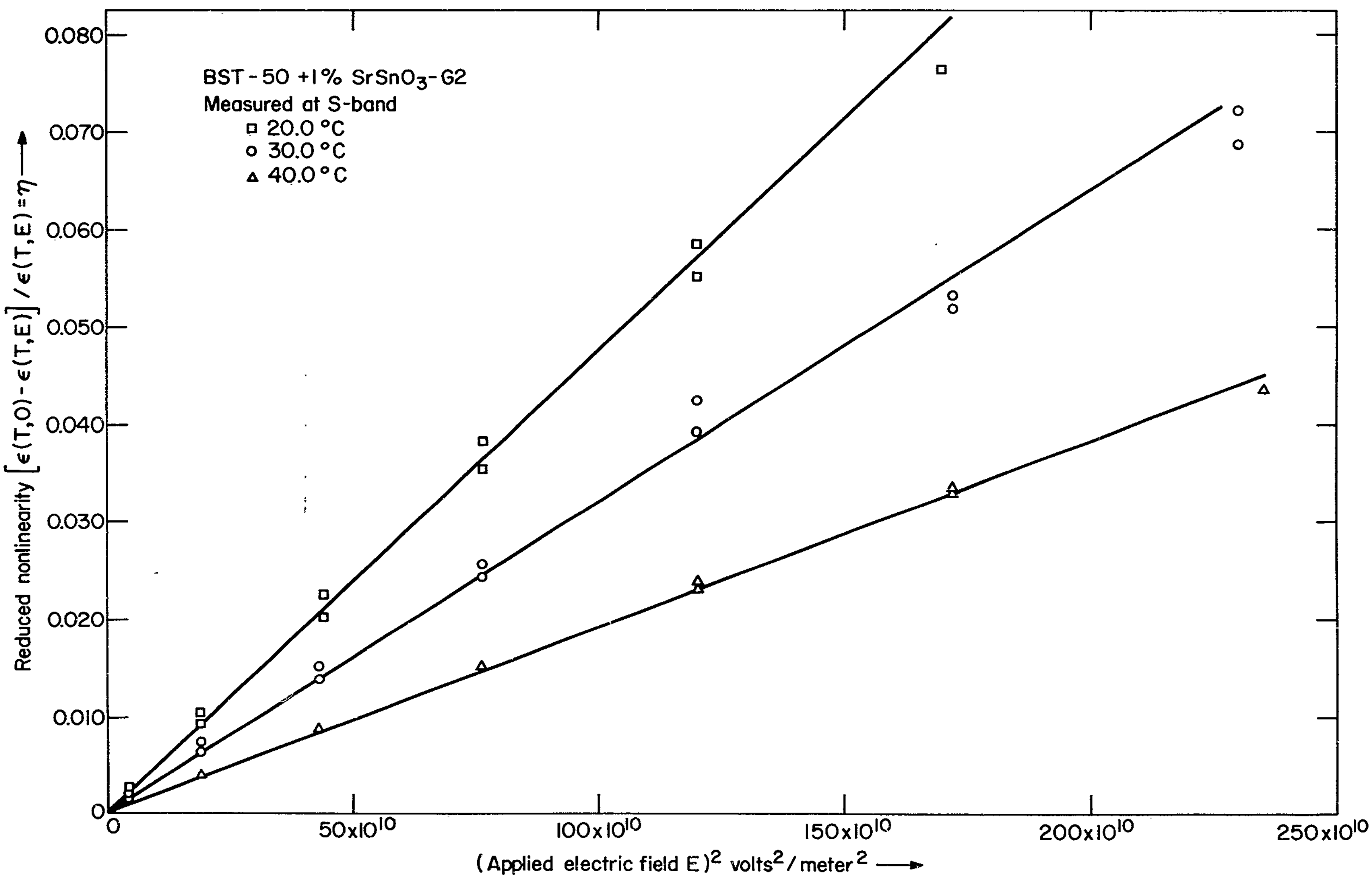

REDUCED NONLINEARITY FOR BST-50 +1% $SrSnO_3$-G2 MEASURED AT CONSTANT TEMPERATURE

FIGURE 8

Under conditions where Eq. (1) is valid the graphs would be straight lines but a noticeable concave down curvature is present in most of them. Taking an average slope up to values of E^2 equal to 10^{12} $\text{volts}^2/\text{metre}^2$ we can calculate values for the coefficient A which are summarized in Table III.

TABLE III

Material	Temp (°C)	A °K m^2/V^2
BST-50 + 1% $SrSnO_3$-B1	40.0	3.16×10^{-18}
	30.0	2.73×10^{-18}
	21.7	2.14×10^{-18}
BST-50 + 1% $SrSnO_3$-G2	40.0	0.837×10^{-18}
	30.0	0.925×10^{-18}
	20.0	0.850×10^{-18}

4.2 Loss Tangents of Stannate Doped BST-50 Samples

Loss Tangents for stannate doped BST-50 samples C and G have been measured in the temperature range 300 - 500°K by the usual technique of measuring the half width of dielectric cavity resonances observed in a spherical sample. The measurements were done at K-band and the results are plotted in Fig. 9 together with the data already reported for the material B.[6]

4.3 Low-frequency Dielectric Constants and Nonlinearity of Stannate Doped BST-50 Samples

Figure 10 plots dielectric constant as a function of temperature in the range 200 - 300°K for the stannate doped BST-50 materials B and C. The data was obtained from measurements of the capacity of an electroded parallel plate sample of known geometry. The capacity measurements were done using a 100 kc/s bridge.

---

[6] See Fig. 9, Report No. 9 of this series.

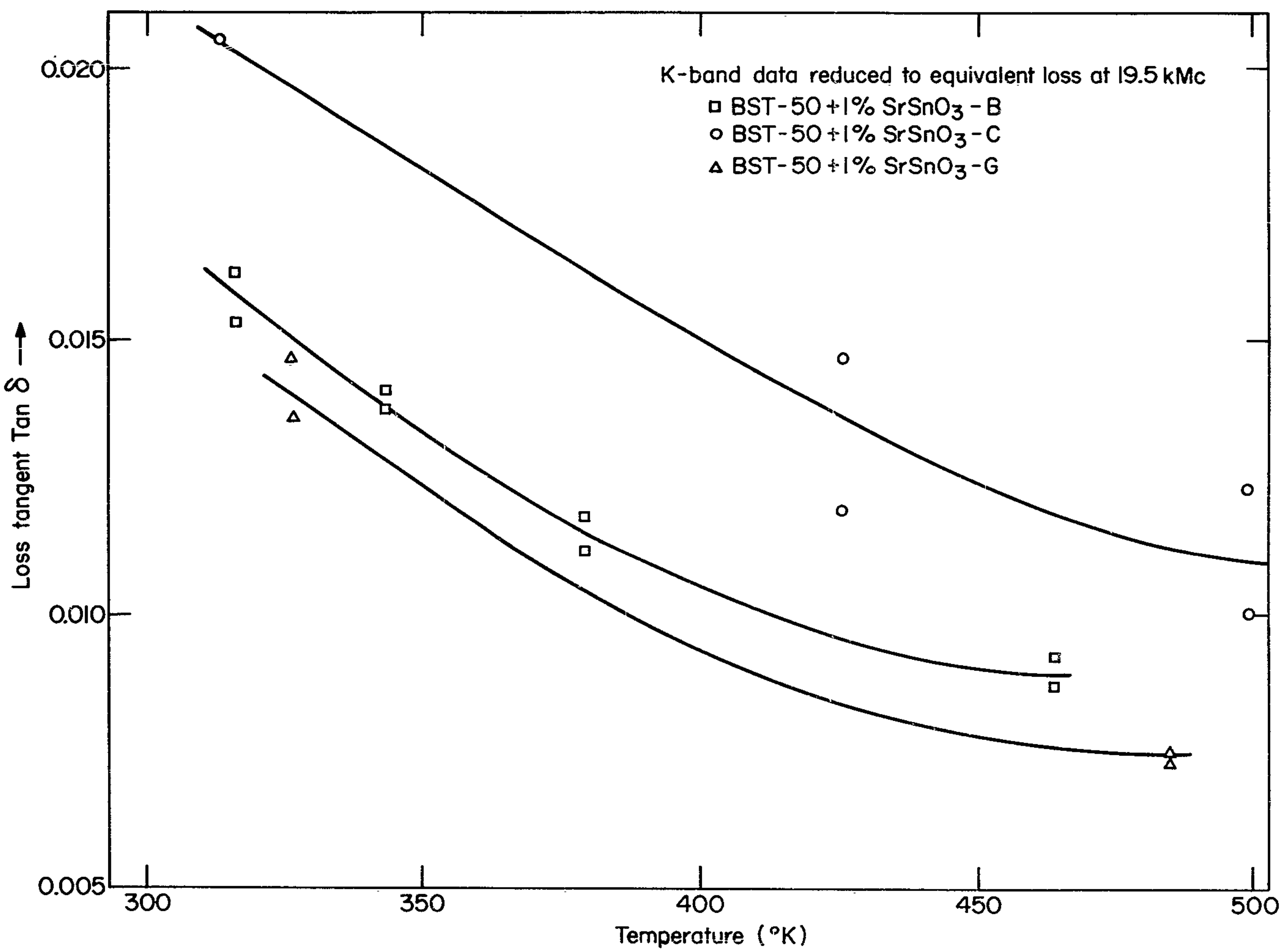

LOSS TANGENT VS TEMPERATURE FOR BST-50 +1% $SrSnO_3$. SAMPLE 5

FIGURE 9

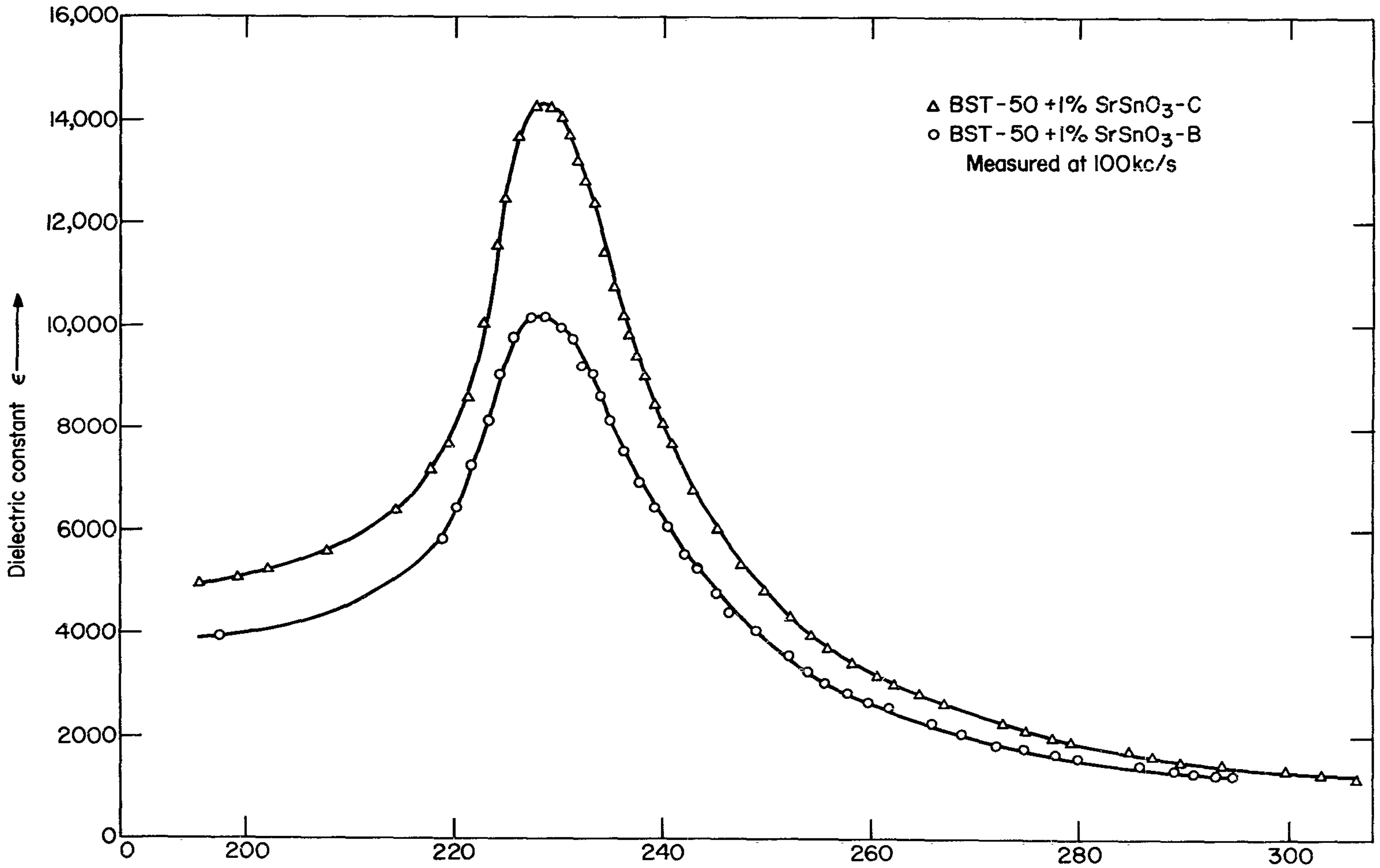

DIELECTRIC CONSTANT VS TEMPERATURE FOR BST-50 +1% $SrSnO_3$ MATERIALS

FIGURE 10

The nonlinearity was measured for both samples B and C by using the bridge to measure the incremental capacity of the sample while a dc voltage was maintained across it. The dc voltage is, of course, blocked from the bridge by coupling condensers with capacities greatly in excess of the sample capacity.

The results for sample B are plotted in Fig. 11 in the form of the reduced nonlinearity η vs E^2 at various temperatures in the range -15 – 40°C. The data does not fall on straight lines but a nonlinearity coefficient A can be estimated using an average slope of the curves below $E^2 = 7.5 \times 10^{11}\ V^2/m^2$.

The results of this analysis for B are presented in Table IV together with similar results for C calculated from unplotted data.

TABLE IV

Material	Temp (°C)	A °K m^2/V^2
BST-50 + 1% $SrSnO_3$-B	40.0	2.29×10^{-18}
	24.6	2.37×10^{-18}
	1.0	1.325×10^{-18}
	-12.6	0.970×10^{-18}
BST-50 + 1% $SrSnO_3$-C	13.2	0.700×10^{-18}
	3.2	0.763×10^{-18}
	-7.1	0.855×10^{-18}

4.4 The Preparation and Microstructure of the Stannate Doped BST-50 Materials

Although the measurements on BST-50 + 1 % $SrSnO_3$ - B as quoted in the previous report seemed to indicate a good material it has proved rather difficult to reproduce its properties in the first repeat batches which we attempted to make, e.g., sample C.

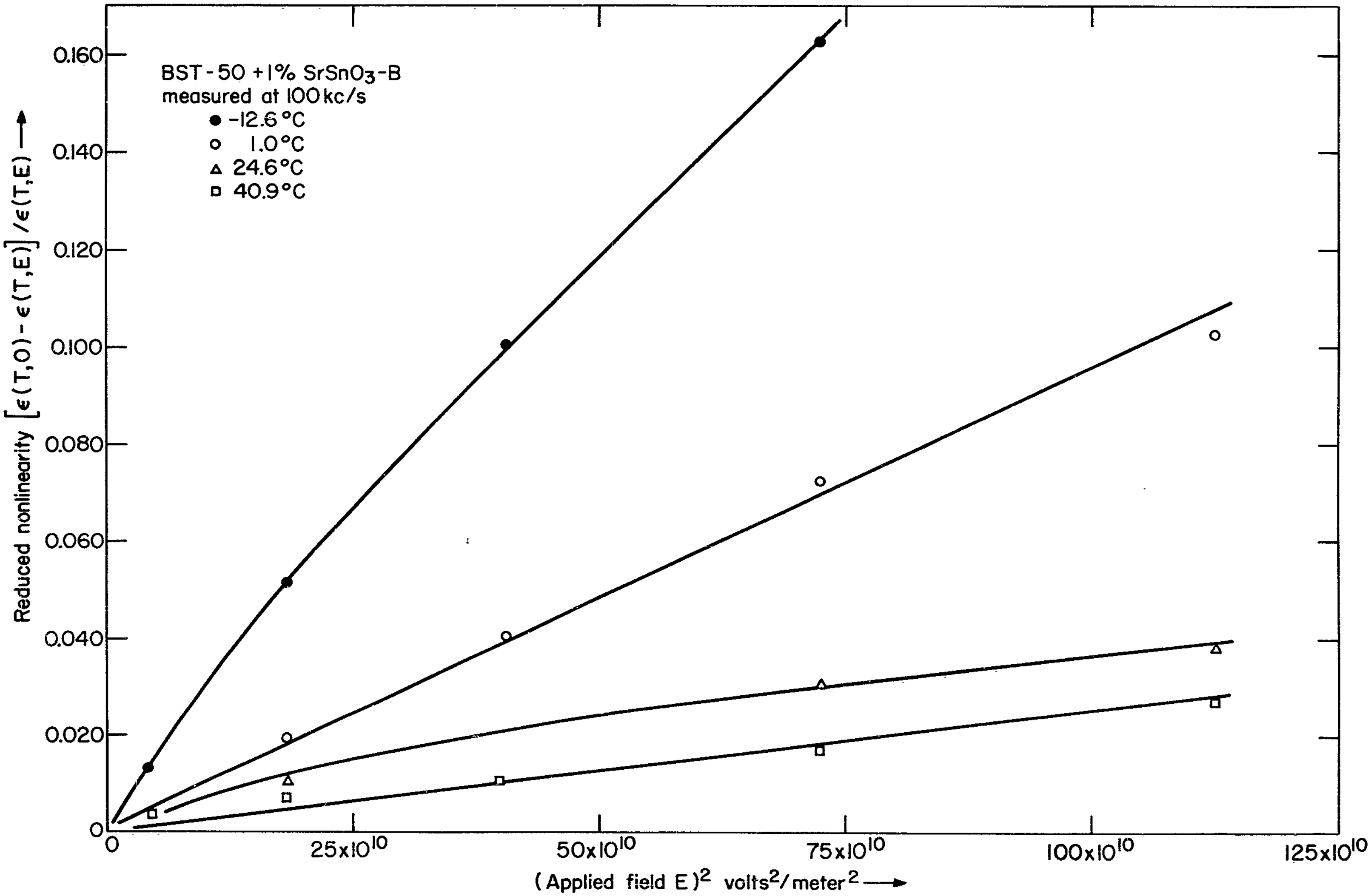

REDUCED NONLINEARITY FOR BST-50 +1% $SrSnO_3$-B NEAR THE CURIE TEMPERATURE

FIGURE 11

For this reason we tabulate the processing conditions for the various samples made to date and give photomicrographs of polished, etched samples of the various materials in Figs. 12, 13, and 14.

In connection with the data of Table V it may be added that the theoretical density of the material is 5.61 and that the measured densities were established by weighing accurately measured cubes.

TABLE V

SUMMARY OF BST-50 + 1% $SrSnO_3$ PROCESSING								
Sample	Batch Wt (g)	Milling Time (hr)	Calcine 1150°C (hr)	Milling Time (hr)	Firing Rate	Firing Temp (°C)	Firing Soak (hr)	Sample Density
A	25	14	1	4	200°/hr	1400	2	---
B	25	10	---	---	200°/hr	1400	2	5.11
C	25	4	---	---	200°/hr	1400	2	5.16
D	25	10	---	---	200°/hr	1400	2	---
E	25	10	---	---	200°/hr	1400	2	5.11
F	225	10	---	---	50°/hr	1400	1	---
G	100	10	4	10	50°/hr	1400	1	5.29
H	250	75	---	---	50°/hr	1400	1	5.12
I	100	75	4	10	50°/hr	1400	1	5.18

4.5 The Dielectric Constant and Loss Tangent of Hafnate Doped BST-50 Samples

Materials of the composition $Ba_{0.5}Sr_{0.5}O_3$ + 1% $BaHfO_3$ and $Ba_{0.5}Sr_{0.5}O_3$ + 2% $BaHfO_3$ were prepared using zirconia free hafnate and milling and calcining several times at low temperature is the manner previously reported.[7]

---

[7] Section 4.94, Report No. 9 of this series.

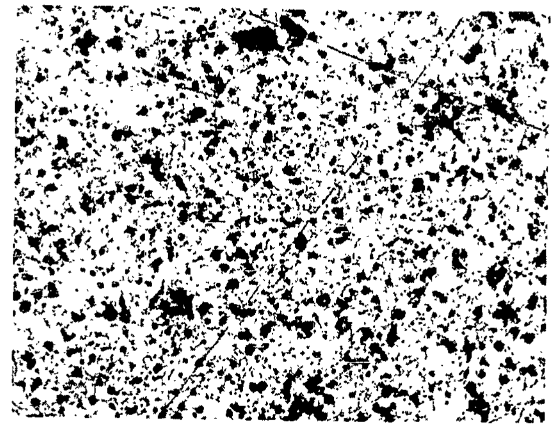

B
100μ

(a)

C
100μ

(b)

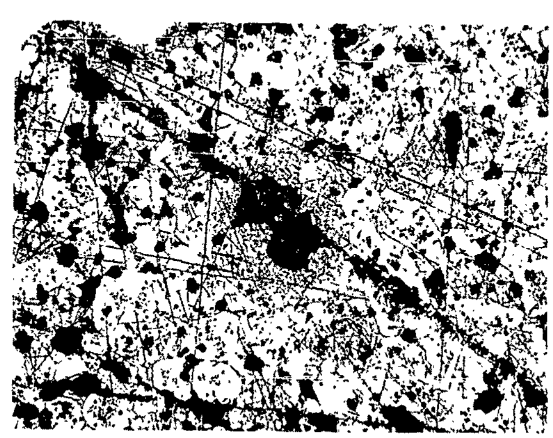

E
100μ

(c)

FIGURE 12

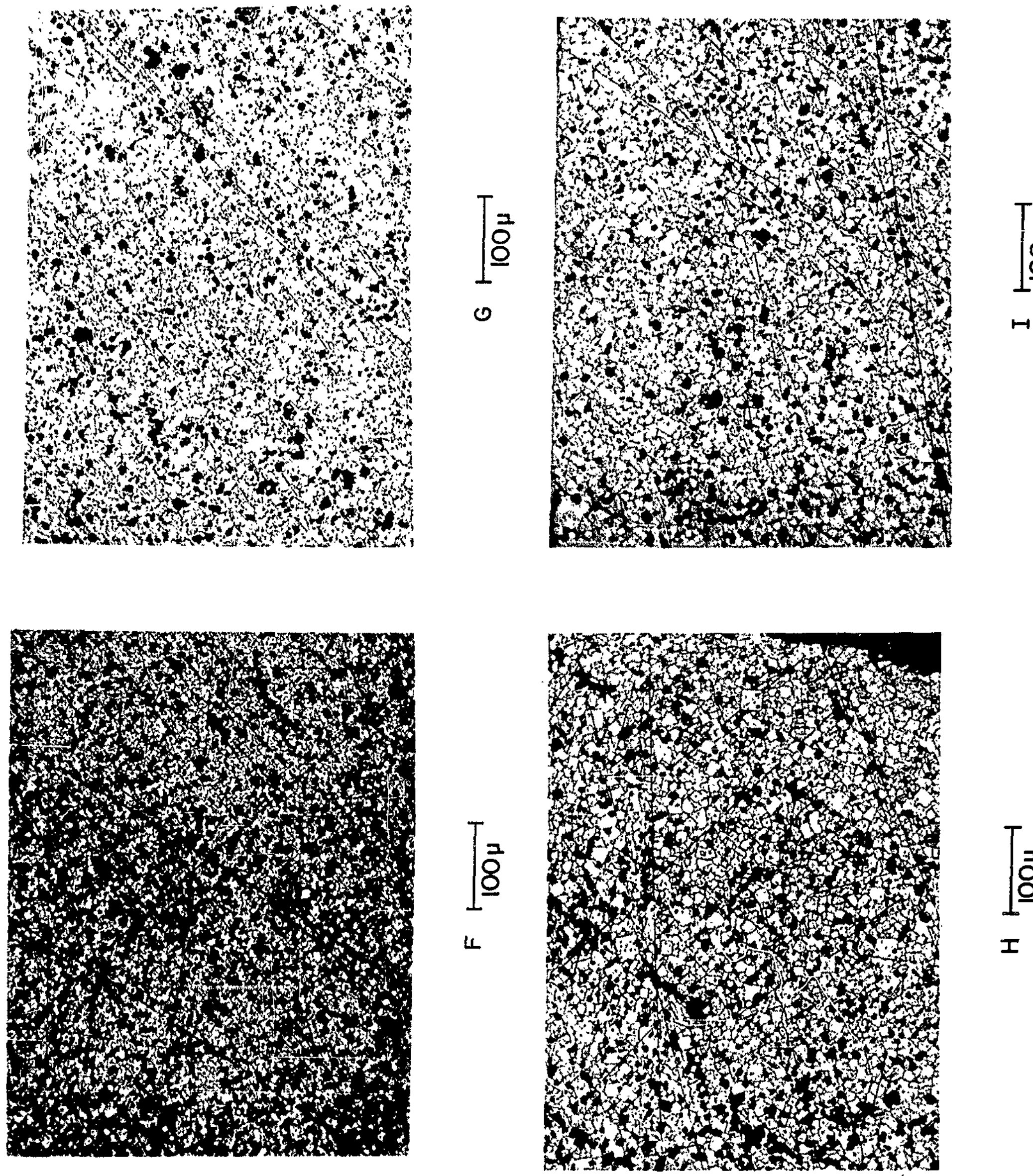

FIGURE 13

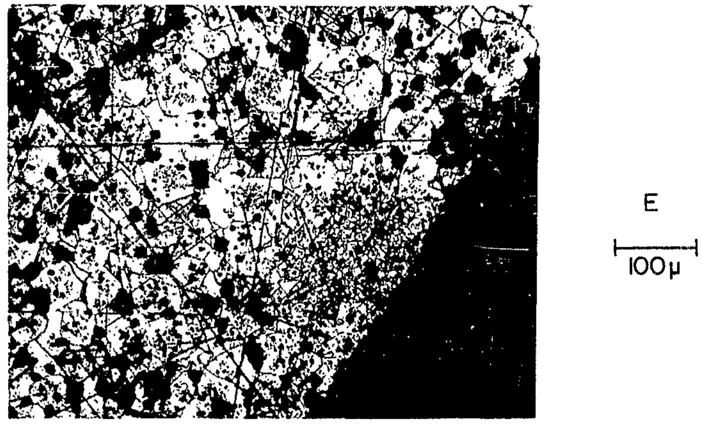

(a)

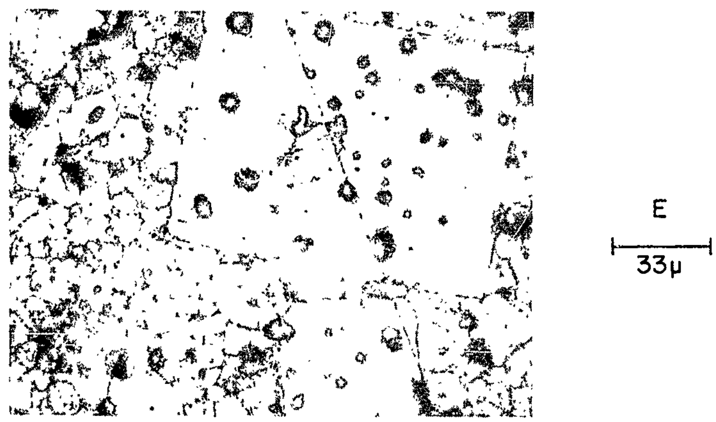

(b)

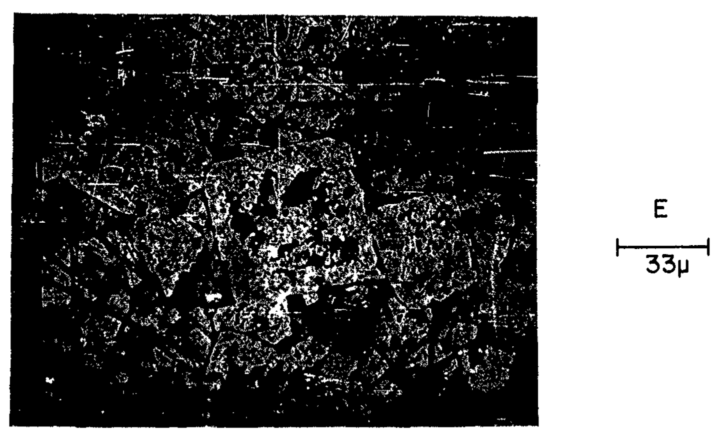

(c)

FIGURE 14

The dielectric constant and loss tangents were measured by observing the frequency and half width of dielectric cavity resonances in sample spheres by the usual microwave technique at K-band.

The dielectric constants are plotted in Fig. 15 as a Curie plot in the temperature range 300 – 500°K and can be analyzed to give the results summarized in Table VI.

TABLE VI

Material	T_c°K	C
BST-50 + 1% $BaHfO_3$	242	7.52×10^4
BST-50 + 2% $BaHfO_3$	242	7.50×10^4

The loss tangent data is plotted over the same temperature range in Fig. 16 together with typical values for good quality pure BST-50.

4.6 Dielectric Constant and Loss Tangent for $Cd_2Nb_2O_7$ Ceramic

The dielectric constant and loss tangent of ceramic cadmium niobate were measured by the usual dielectric resonance technique at X-band.

Figure 17 gives the dielectric constant data as a Curie plot over the range 210 – 550°K and can be analyzed over the central linear portion to indicate T_c = 165°K and C = 7.54×10^4.

The loss tangent measured of X-band was transformed to the equivalent value at 20.0 kMc/s assuming tan δ is proportional to frequency. The results are plotted in Fig. 18 over the temperature range 250 – 450°K.

4.7 Measurement of Field Dependent Loss and Nonlinearity in BST-50

4.7.1 Apparatus and Procedure

A technique was previously described[8] for the measurement of field dependent loss in $SrTiO_3$. This method had advantages over earlier

---

[8]Section 4.3, Report No. 8 of this series.

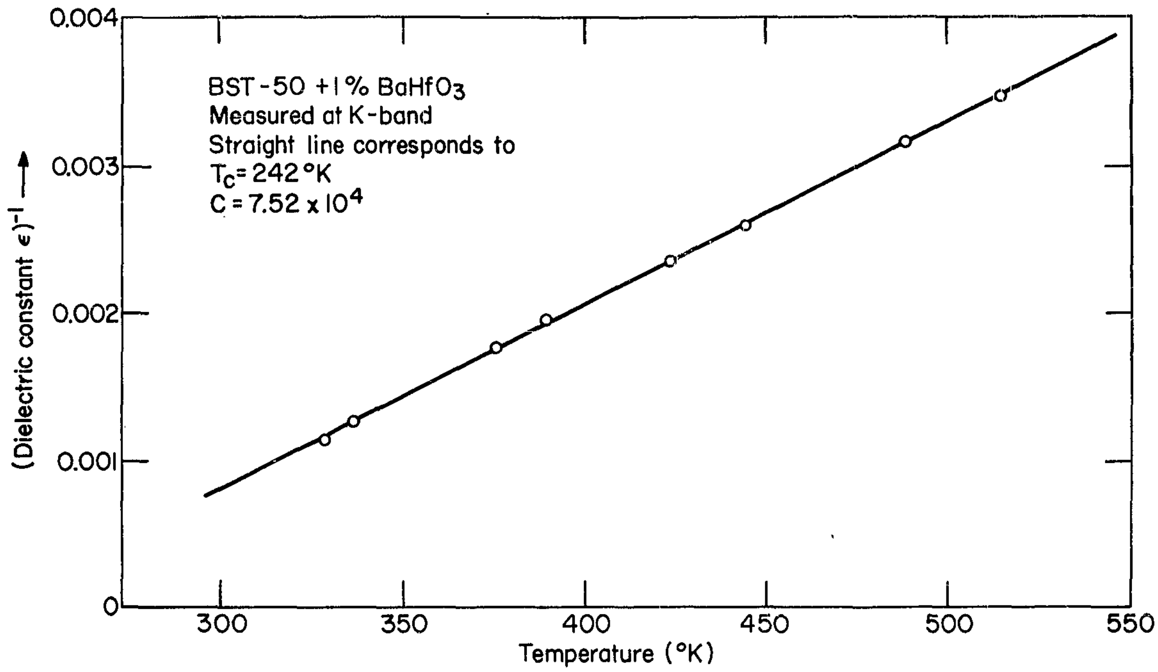

a) CURIE PLOT OF DIELECTRIC CONSTANT VS TEMPERATURE FOR BST-50 +1% $BaHfO_3$

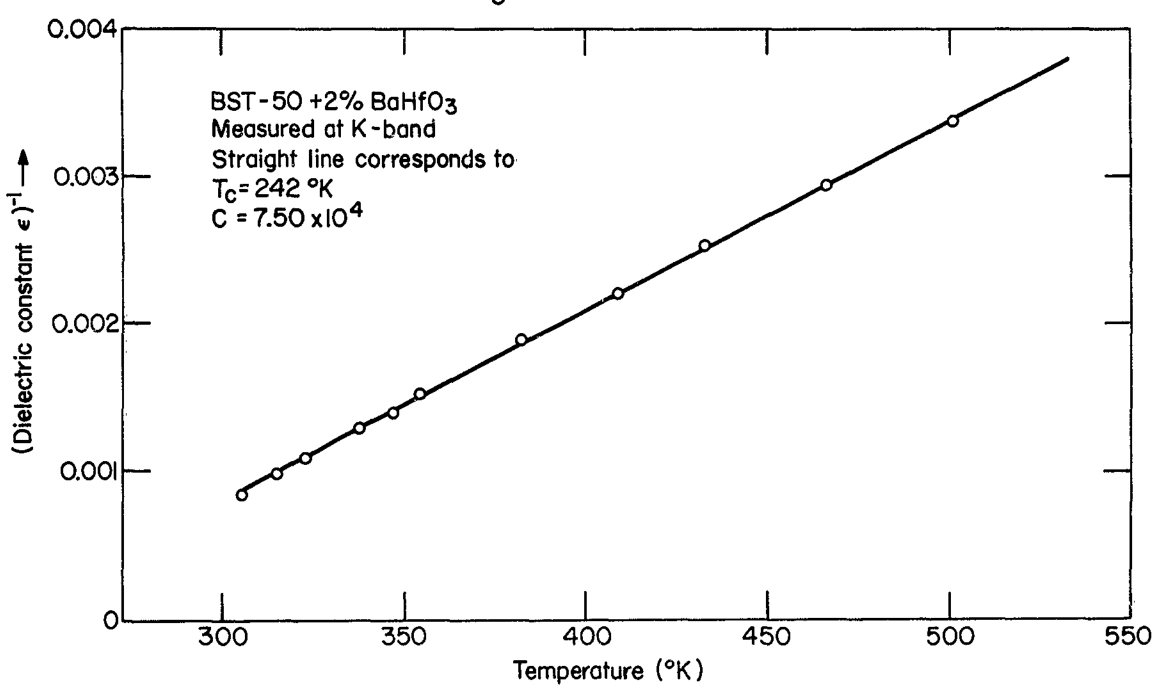

b) CURIE PLOT OF DIELECTRIC CONSTANT VS TEMPERATURE FOR BST-50 +2% $BaHfO_3$

FIGURE 15

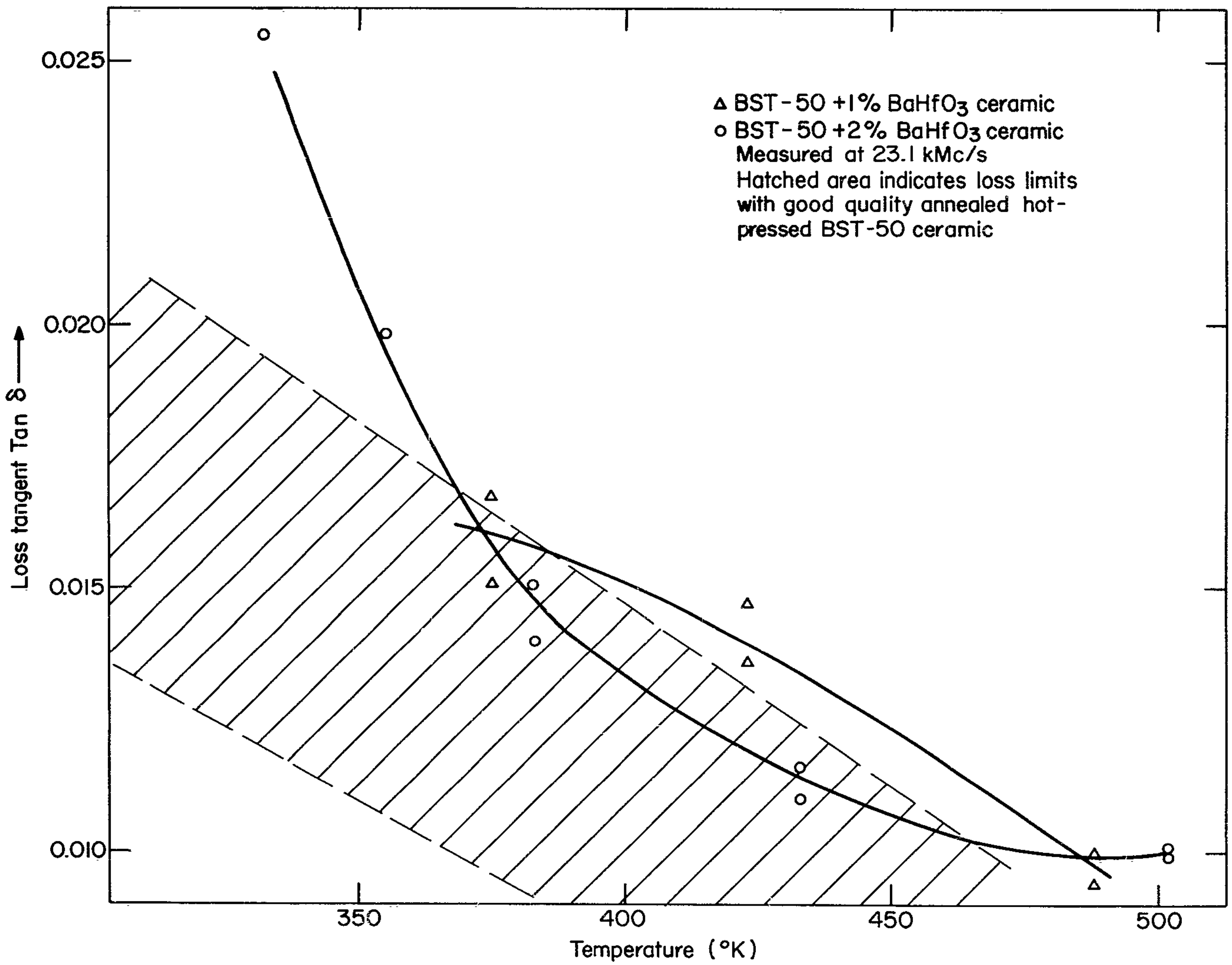

LOSS TANGENT VS TEMPERATURE FOR BST-50 DOPED WITH $BaHfO_3$

FIGURE 16

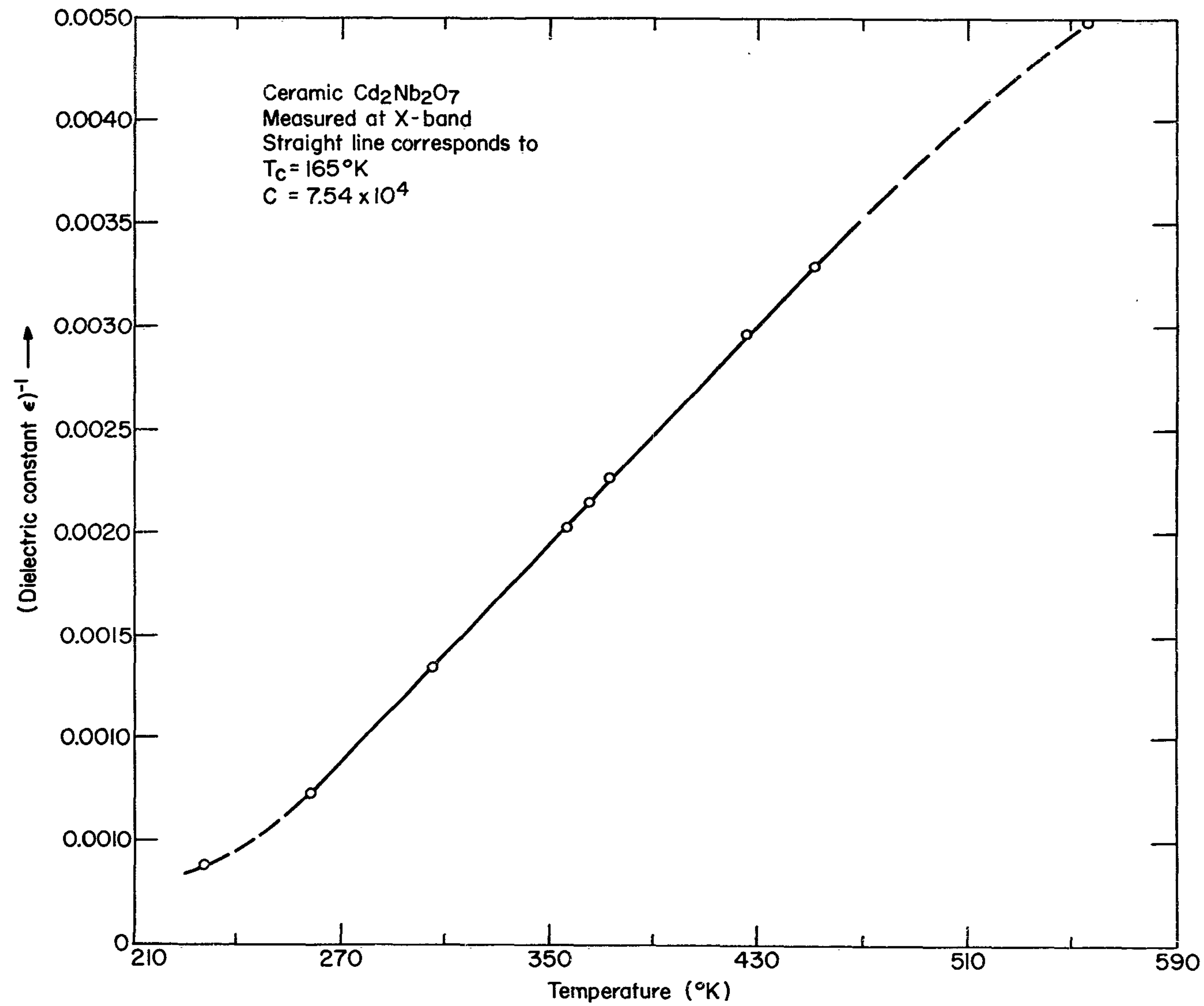

CURIE PLOT OF DIELECTRIC CONSTANT VS TEMPERATURE FOR CERAMIC $Cd_2Nb_2O_7$

FIGURE 17

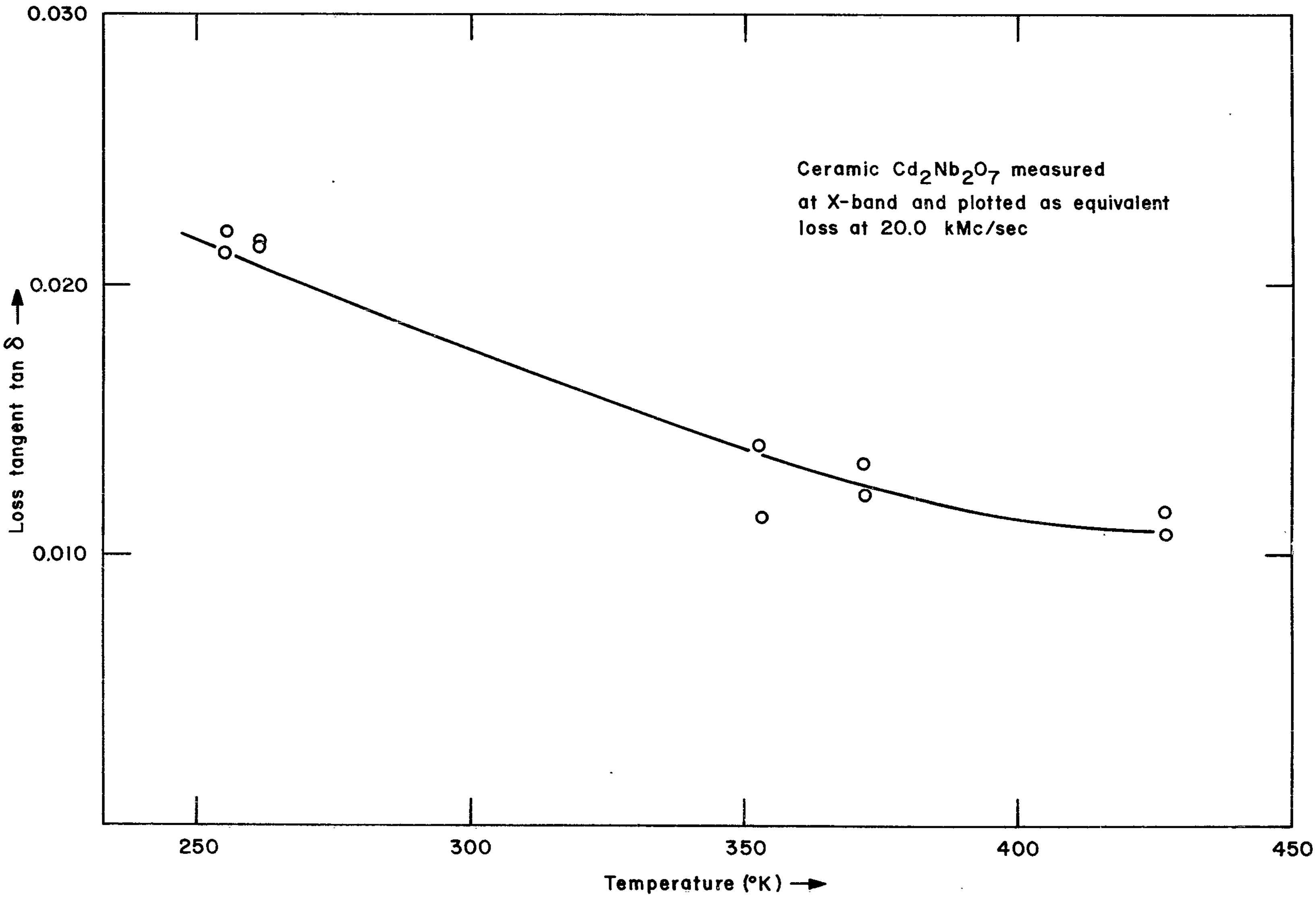

LOSS TANGENT VS TEMPERATURE FOR CERAMIC $Cd_2Nb_2O_7$

FIGURE 18

attempts which were explained in the reference quoted.[8] There remained a serious disadvantage; the intrinsic loss of the sample only accounted for about 10 percent of the value deduced from the observed Q. At the time of the previous measurement it was assumed that the extra loss could be attributed to skin loss and this assumption permitted the data to reduced to the desired experimental form.[9]

Subsequent calculation suggested that the skin loss could not be large enough to account for the small Q observed in the resonant electroded strip lines formed by the samples used in coaxial structures at S-band. The Q observed was in fact depressed by the fact that the strip lines were tightly coupled to the coaxial line. The coupling, and its dependence on dielectric constant (and hence upon applied field) were not quantitatively or qualitatively understood and so the "corrections" referred to in reference 9 are almost certainly incorrect. The results are therefore in question. For this reason among other reasons it was decided to conduct the field-dependent loss measurements in waveguide structures where the sample is very poorly coupled to the guide so that the observed Q is indeed the genuine Q of the dielectric resonator.

The apparatus is indicated in schematic form in Fig. 19a. It consists of an X-band microwave bridge containing a temperature stabilized sample mounted in one arm in the fashion illustrated by Fig. 19b. Reflected signals from the sample and other components in the same arm of the bridge pass into the balancing arm of the bridge and can normally be cancelled to zero by suitable adjustment in the compensating arm of the bridge. The crystal in the balancing arm of the bridge will then detect a zero signal which will be passed to the ratio meter. A slight tuning of the source, sufficient to bring it onto a sample resonance, will result in an enhanced reflection from the resonant sample; an out of balance signal in the balance arm, and a non-zero signal being passed to the ratio meter from the crystal detector. The ratio meter receives its other input from a crystal detector sampling the power

---

[9]See Eq. (6) and Fig. 5 of Report No. 8 of this series.

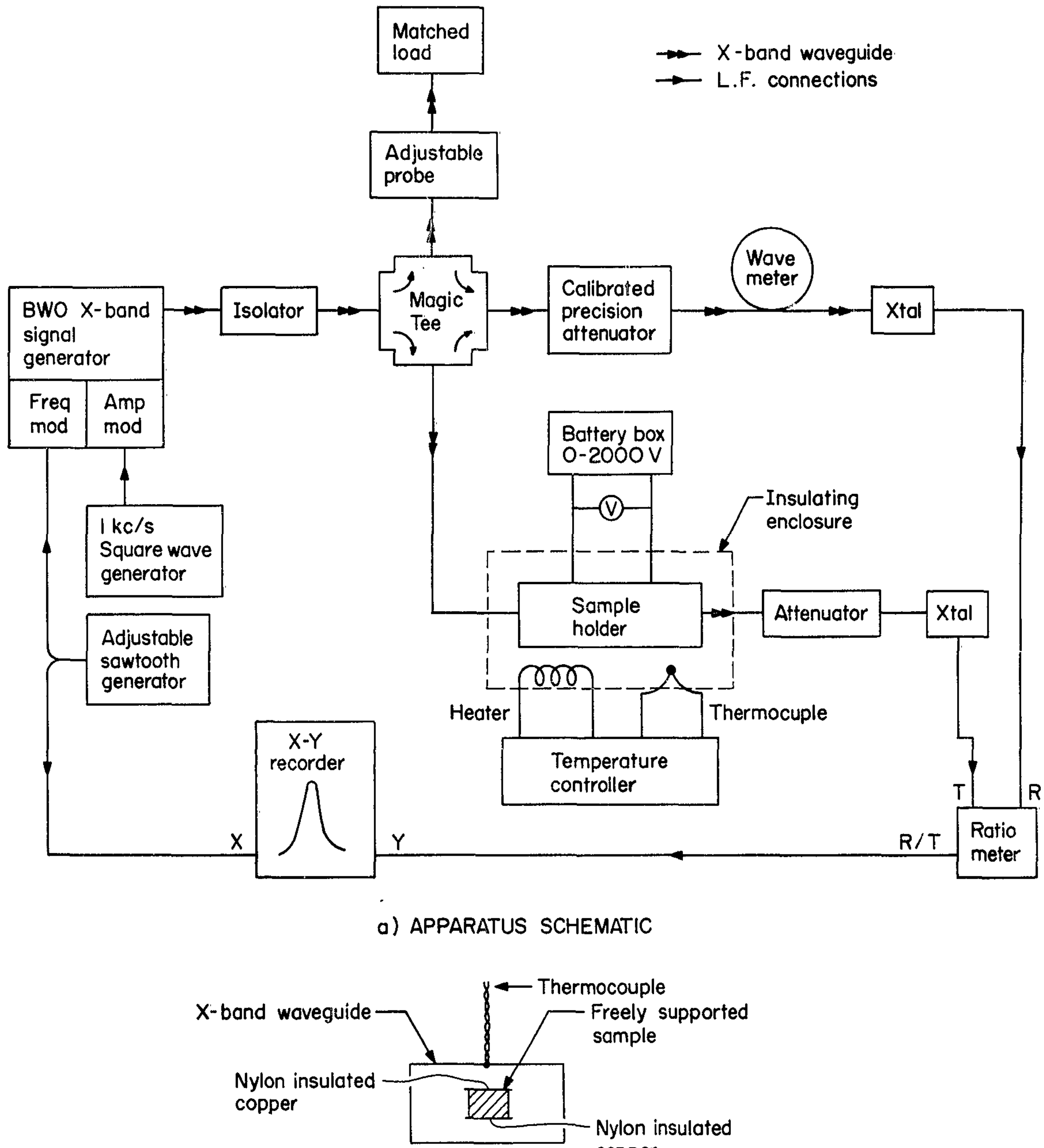

a) APPARATUS SCHEMATIC

b) CROSSECTION OF SAMPLE HOLDER

APPARATUS FOR MEASUREMENT OF FIELD DEPENDANT LOSSES AT X-BAND

FIGURE 19

level of the whole system and so the output of the ratio meter is proportional to the strength of the resonant reflection coefficient and independent of fluctuations of power level to a considerable extent.

In operation the X-band source is scanned in frequency slowly, automatically and continuously. The sawtooth generator responsible for the frequency modulation of the BWO X-band signal generator also drives the X component of an X-Y recorder which displays the ratio meter output on its Y-axis. The X-Y recorder therefore draws directly, a graph of reflection characteristic vs frequency; and from this the resonant frequency and half width can be obtained by straightforward measurement.

The frequency scale must be calibrated by two frequency measurements (preferably close to the resonance) using the wavemeter included in the apparatus and, of course, the frequency scan may be halted at any chosen point for this purpose. In addition the vertical scale of the graph may be checked for linearity of the crystal detectors (as power detectors that is) by imposing known steps of attenuation in the bridge balance arm. A calibrated precision attenuator is included in the schematic for this purpose but this check need not be performed for every experiment – it suffices to repeat it if and when the detector is changed or if there is any major change in detected power loads.

The equipment operates at power loads from 20 – 100 mw and scans over the frequency range 8 – 12.5 kMc/s. The samples are approximately $5 \times 1.5 \times 0.5$ mm ground and polished parallel to better than one percent. The electrodes are applied by chemically depositing silver and following this with electroplated copper. Without any effort at temperature stabilization the section of waveguide within the insulating enclosure remains at constant temperature within 0.25° at 150°C. The sample temperature, judged from the frequency stability of its resonance is of approximately the same magnitude. Although it is possible to add temperature stabilization to maintain the waveguide temperature more constant, preliminary efforts show that the sample temperature cannot be better stabilized unless its thermal contact with the stabilized waveguide is improved. This stability sets a lower limit on the accuracy with which peak widths can be measured and hence a lower limit upon the field dependent loss which can be observed (see 4.7.3).

4.7.2 Skin losses

The Q_s of a cavity subject only to skin losses can be expressed as[10]

$$Q_s = \frac{2 \int_v H^2 dV}{\int \Delta\, H_s^2\, dS} \quad . \tag{7}$$

where

$\underline{H}$ is the field at any point in the cavity

$\underline{H}_s$ is the field at a point on the surface of the cavity

Δ is the effective skin depth which can be written

$$\Delta = \sqrt{\frac{2}{\omega \mu_s g_s}} \quad . \tag{8}$$

where

ω is the angular frequency

μ_s is the permeability of the wall material

g_s is the conductivity of the wall material.

The expression in Eq. (7) becomes very simple for an H_{10n} mode in a rectagular parallelpiped which has lossy boundaries on the y = constant boundaries only, i.e., for our resonant samples in their simplest resonance. The simplification comes about since there is no y dependance of the magnetic field. The integral in the numerator can be integrated with respect to

---

[10] Any standard microwave textbook, e.g., H. M. Barlow and A. L. Cullen, "Microwave Measurements," p. 79, Constable, London 1950.

the y variable and the remaining integrals in numerator and denominator are identical. Then we have

$$Q_s = \frac{b}{\Delta} \qquad . \tag{9}$$

Where b is the thickness of our sample in the y-direction, i.e., thickness between electrodes.

Taking $g_s = 6 \times 10^7$ mhos/meter cube and $\mu_s = 4\pi \times 10^{-7}$ we can evaluate Q at 10 kMc/s as

$$Q_s = \frac{b}{0.656 \times 10^{-4}} \qquad . \tag{10}$$

The experimental sample used for the measurements reported below had b equal to 0.061 cm and we therefore anticipate a contribution to the measured tan δ which would appear to be of magnitude 1.075×10^{-3} at 10 kMc/s.

The Q and apparent tan δ for a sample of BST-50 was measured in the X-band setup of Section 4.7.1 without electrodes, with very thin transparent evaporated tin electrodes, with thick opaque evaporated tin electrodes and with the silver and copper electrodes previously described.

The results are summarized in Table VII.

TABLE VII

Electrodes	Temp of Measurement (°C)	Resonant Frequency (kMc)	Expt tan δ	Intrinsic tan δ	Skin Loss	
					Expt tan δ	Calc tan δ
No Electrodes	110.5	11.100	7.7×10^{-3}	7.7×10^{-3}	0	0
Thin Evap. Tin	98.0	11.525	8.58×10^{-3}	8.69×10^{-3}	---	---
Thick Evap. Tin	127.0	8.380	7.05×10^{-3}	5.25×10^{-3}	1.80×10^{-3}	1.18×10^{-3}
Silver and Copper	179.5	9.875	6.1×10^{-3}	4.75×10^{-3}	1.35×10^{-3}	1.08×10^{-3}

In connection with the table above it must be mentioned that column 5 has been calculated using a well-established expression[11]

$$\tan\delta = \frac{f}{T-T_c} \cdot \frac{a}{20} \qquad . \tag{11}$$

Where f is the frequency of the resonance in kMc/s, and T its temperature. T_c was taken as 227°K and $a = 2.17$ to be consistent with known data for the material under experiment.

4.7.3 Field dependent losses in BST-50

The BST-50 sample with leads attached was mounted in the manner indicated by Fig. 19b in the apparatus described in Section 4.7.1. Resonances were traced out with zero field and at a field of 1.64×10^6 volts/metre. The resonances are illustrated in Fig. 20 which gives their center frequencies and frequency half widths. A broadening of the half-power width by approximately five percent was observed when the field was applied but the 0.25°C temperature stability implies that the resonant frequencies are only stable to about one part in 2000. At this frequency that means stable to 0.005 kMc/s which is the extent of the half-power broadening in frequency. We are therefore only able to conclude that for BST-50 at 151°C the increased loss produced by a field 1.64×10^6 volts/metre. is expressible as

$$\tan\delta_E = (\tan\delta)_E - (\tan\delta)_o \leq 1.2 \times 10^{-3} \qquad .$$

In assigning this upper limit we have added the observed increase in loss tangent to the worst possible apparent decrease in loss tangent that could have arisen from the temperature instability.

The peak shift observed in the data presented in Fig. 20 can also be used to calculate a value for the nonlinearity coefficient A. Taking T to be 151°C, $\epsilon = 425$, and $C = 7.47 \times 10^4$ for this sample of BST-50 we calculate $A = 5.0 \times 10^{-18}\ ^\circ\mathrm{K\,m^2/V^2}$.

---

[11] G. Rupprecht, R. Bell, and B. D. Silverman, Phys. Rev. 123, 97 (1961), and Fig. 5, Report No. 7 of this series.

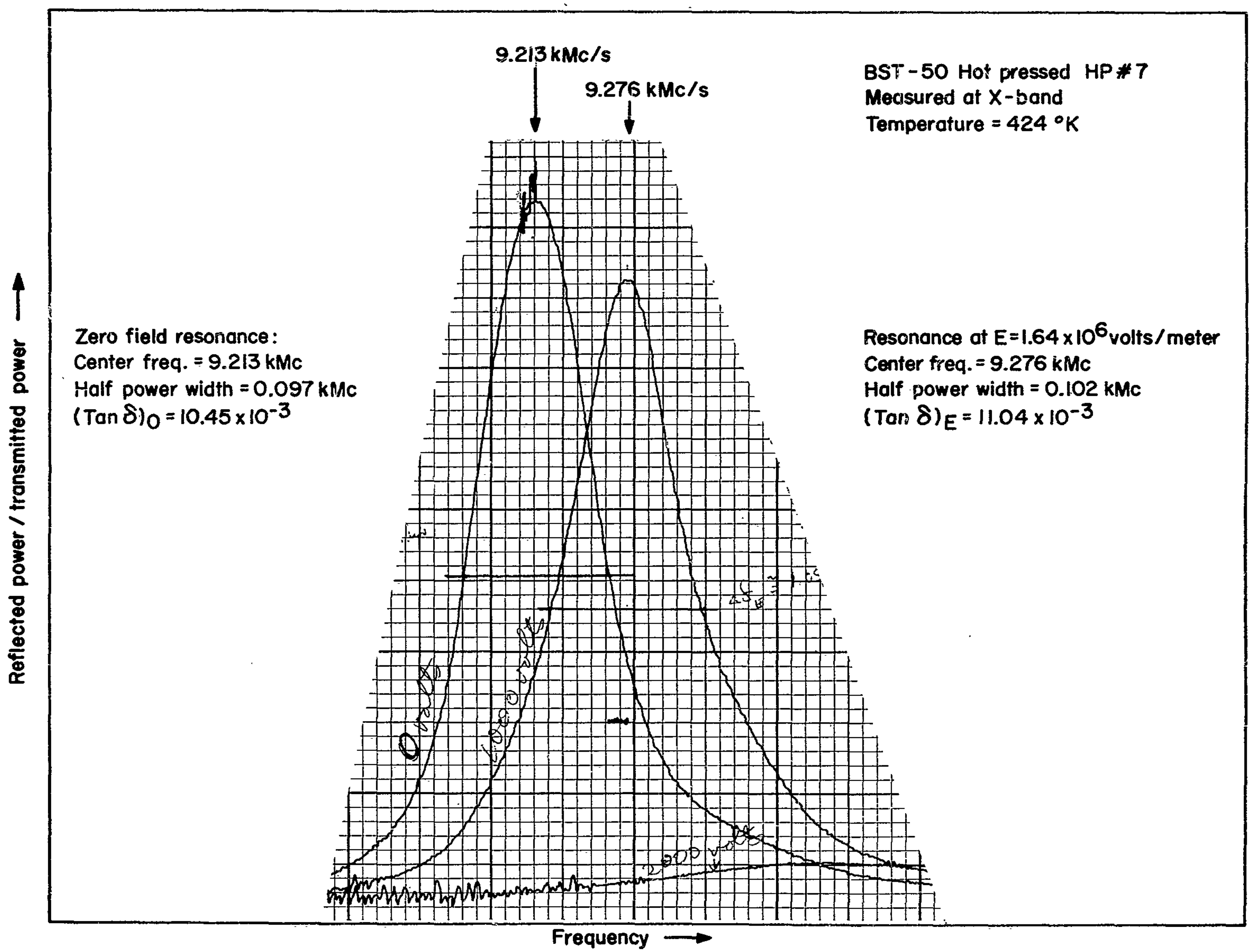

FIELD DEPENDANT LOSS IN BST - 50
FIGURE 20

4.8 Time Stability of Dielectric Constant in BST-50 + 1% $SrSnO_3$-B1

The lack of stability of dielectric constant for ferroelectric materials in the presence of an electric field has been commented on by many authors. The data of Fig. 21 give some quantitative information upon the magnitude of this effect in a sample of stannate doped BST-50. The figure shows the dielectric constant falling by about 1.7 percent over the course of an hour at 40°C and with a field of 10^6 volts/metre.

The effect in this sample is thought to be comparable with that in other samples of doped and pure BST-50.

5. CONCLUSIONS

5.1 The Stannate Doped BST-50 Materials

The encouragingly high nonlinearity coefficient and low loss tangent found previously[1] in BST-50 + 1% $SrSnO_3$-B1 have prompted the production of many more samples of the same material in order that we might establish reproducible production precedures and obtain reproducible results.

We will first discuss the results of measurements on some of these materials and leave discussion of the materials themselves until later.

Turning to the experimental data of Section 4.1.1 we see that the dielectric constants of new samples C and G have been measured together with those for a second portion of the former sample B. The portion B2 is very similar to the previously measured piece B1. B2 has a slightly higher Curie constant and a slightly lower A coefficient that B1 had but it is still far from being a typical BST-50. In contrast the samples C and G are almost indistinguishable from normal BST-50 as the data of 4.1.1 and 4.1.3 show.

The discrepancy in Curie constant between samples B, C, and G deserves some comment. The sample densities are quoted in Section 4.4 and we may make due allowance for the effect of density on dielectric constant and hence Curie constant.

Lewin[12] gives a formula for the bulk dielectric constant of a "loaded dielectric." When applied to our porous dielectrics his formula may be simplified to

$$\epsilon = \epsilon_1 \left[1 - \frac{3f}{2-f} \right] \quad . \tag{12}$$

---

[12] L. Lewin, "Advanced Theory of Waveguides," p. 156 Iliffe, London (1951).

Where

ϵ = observed dielectric constant of the porous material

ϵ_1 = actual dielectric constant of the dense material

(1-f) = density of the porous material relative to the theoretical density.

Using this formula we should expect the Curie constants of B, C, and G to be in the ratio 1.00:1.02:1.06 whereas they are in fact in the ratio 1.00:1.09:1.17. We are entitled to conclude that they differ in constitution and presume that the difference may be in the way that the Sn impurity has been incorporated.

When materials have different Curie constants, dielectric constants, and Curie temperatures the comparison of nonlinearity cannot truly be made by merely comparing the nonlinearity coefficient A. It was pointed out in the previous report that the four-fold increase in coefficient A was in part a reflection of the rather low dielectric constant found in the piece B1.

The fact that there is a genuine difference in the nonlinearity of B2 and C1 can be observed in the scale of temperature shifts indicated in Figs. 4 and 5 but the difference is much more directly evident when the data is replotted as in Fig. 6.

The y-coordinate of Fig. 6 is essentially a measure of $\Delta\epsilon/\epsilon$ for a specified dc field. This is the quantity which has direct meaning in any engineering application. It is very evident from this graph that the pieces B1 and B2 had a markedly larger nonlinear effect at all but the lowest temperatures. Roughly speaking the reduced nonlinearity appears to be twice that of material C or of pure BST-50 plotted for comparison. The material C itself shows a slight superiority over the pure BST-50 material.

It is fair to point out that the expressions of Eq. 1 and 2 are approximations only valid for small polarization and for materials obeying the Curie law. We maintain that these approximations are valid in temperature regions above 10°C and at fields below 10^6 volts/metre. The extent of curvature in such curves as are presented in Figs. 4 and 5 support this. Even so it is possible to make direct measurement of the reduced nonlinearity by the method described in Section 4.1.3 and obtain data as in Fig. 7 and 8 which are dependent on no justification of Eq. 1 and 2. The data of Fig. 7 and 8 again show sample B1 to have an enhanced nonlinearity in comparison with sample G2.

If the graphs of Fig. 8 are interpolated at $E^2 = 10^{12}$ volts^2/metre^2 one can obtain three points which if plotted on Fig. 6 would lie almost exactly on the curve for the material C. The data for B1 reduced in the same way agrees with the B data in Fig. 6 at 40°C (i.e., $T-T_c = 84.5$) but indicates lower nonlinearity at the lower temperatures.

We conclude there is a definite enhanced nonlinearity in B which we have not reproduced in materials C or G.

The loss data presented in Fig. 9 shows C to be rather a poorly reacted material but indicates G to be slightly better than B, the data for which is plotted here for comparison purposes.

The low frequency data of Fig. 10 emphasises the lower dielectric constant of sample B but enables us to make one very pertinent observation. The area beneath the curve for the B material is appreciably less than the area beneath the C curve. This implies that the reason for B's low peak value is <u>not</u> that B is an inhomogeneous material containing grains with a wide spread of Curie temperatures. Such inhomogeneous materials have lower but wider peaks which total the same area as is found in a more homogeneous sample. The spread of Curie temperatures in each sample can be crudely estimated as the temperature difference between the dielectric constant peak and the point half-way down the low temperature side of the peak. On this basis B has a spread of 6.5° and C a spread of 6.0°.

This data emphasises our previous conclusion that there are constitutional or structural differences between our samples and particularly that B is unusual in its properties.

The low frequency data of Section 4. 3 extends the measurement of reduced nonlinearity down to the Curie point. Microwave data in the same temperature range is difficult to obtain because of the high microwave losses and the high dielectric constant. The data permits us to draw no interesting conclusions but is notable for the linearity of the plots in Fig. 11 for low temperatures and high polarizations. As Table IV indicates the superiority of sample B over C is preserved even in this temperature range.

It is appropriate to discuss the sample preparation and microstructure from the historic viewpoint. Sample A was made as a routine trial and error test while searching for impurities capable of influencing nonlinearity. Promising early results on this sample led us to produce sample B and the preparation techniques were not deliberately changed. As the previous report indicated B, had an apparently greatly increased nonlinearity coefficient. Three batches of material were made next in order to repeat the measurements. These materials C, D, and E were poor in physical appearance being spotty in appearance and having some voids in them. C was chosen as the best of the bunch but as the present report indicates C is a typical BST-50 exhibiting only slightly enhanced nonlinearity and having poor loss characteristics.

Photomicrographs of polished etched surfaces of all samples were prepared and those for B, C, and E are illustrated in Fig. 12. The A and D materials were indistinguishable from E and so have not been reproduced here.

The microstructure of the good sample B is noticeably different from the structure of the other materials. The differences may be categorized as :

1. The grain size in B is smaller than in C and E.
2. The grain size in B is more uniform than in C and E.
3. Large amounts of included pores are found within the grains of C and E whereas the porosity in B is mostly inter-granular.

Measurements on the photomicrographs show B to have a grain size of about 10 microns . The grains of C and E fall mostly in the range 10 – 100 microns . This spread of grain sizes is particularly evident in Fig. 14a. Figure 14b shows an example of exaggerated grain growth in a fashion which is atypical for BST-50 – the cause of this will be discussed later. An example indicating the extent of porosity within the grains is found in Fig. 14c. All these examples are from the E material.

The same disadvantages are present but less emphatically so in the C material.

The exaggerated grain growth referred to in connection with Fig. 14b is of a type commonly found in ceramic systems containing an impurity. It occurs when the impurity is not in solid solution with the main constituents of the ceramic but is concentrated at the grain boundary as a second phase. When we see this type of grain growth we presume the $SrSnO_3$ impurity is not being incorporated in solid solution.

Examination of these photomicrographs suggested that longer milling times and a pre-firing calcination would improve homogeneity and uniformity of grain size. Pre-reacting of the materials and controlled firing rates should influence the porosity included within the grains. Four batches F, G, H, and I were prepared incorporating various of the above suggestions. Table V summarizes the preparation of all samples and Fig. 13 shows photomicrographs of the last four materials. The unfavorable features outlined above seem to have been eliminated from these samples.

As we have seen the G material shows no superior nonlinearity over C and is certainly not like B.

We conclude that the visible structural defects of the previous samples were not responsible for their normal BST-50-like nonlinearity and currently have no evidence to indicate why B is superior.

5.2 The Hafnate Doped BST-50 Materials

Working on the assumption that Hf is a worse match in the BST-50 lattice than is Sn, it was thought possible that Hf might influence nonlinearity more potently than Sn. In accordance with this suggestion, materials with small dopings of $BaHfO_3$ were prepared and measurements on them are reported in Section 4.5.

These measurements are preliminary ones giving us the dielectric constant data and loss tangent. The loss data shows losses a little higher than usual indicating some possible trouble in reacting the hafnate but the materials could not be described as bad.

The nonlinearities remain to be measured.

5.3 The Cadmium Niobate Ceramic

It is thought that experiments to influence the nonlinearity by doping should be conducted in materials other than BST-50. We hope therefore to perform such measurements in $Cd_2Nb_2O_7$ and the current measurements are merely to establish a basis for comparison. The measurements so far concluded include only the dielectric constant and microwave loss tangent data as presented in Section 4.6.

5.4 The Field Dependent Losses and Nonlinearity in BST-50

The field dependent losses in $SrTiO_3$ have previously been shown to produce a considerable increase in loss compared with the zero field intrinsic loss in this material. For instance, Report No. 8 of this series points out in Section 5.3 that by applying a field sufficient to produce a 30 percent decrease in dielectric constant at 77°K one enhances the loss tangent tenfold.

This property is a severe obstacle to the use of $SrTiO_3$ in low loss microwave components even under refridgerated conditions.

It would appear from Silverman's analysis of the loss mechanisms in impure systems[13] that the losses in BST-50 arise almost exclusively from the huge amount of "impurity" that is constituted by the 50 percent Ba in a $SrTiO_3$ lattice. There is little reason to expect this impurity loss to be a field dependent one in contrast to the marked field dependence to be expected for those losses arising from the anharmonic lattice forces.

Because of the considerable practical interest in BST-50 we have attempted to measure the field dependent loss in this material. The experiment was done at elevated temperature where the impurity loss is somewhat diminished and any field dependent loss rather increased.

Within the limits of experimental error we could only assign an upper limit to the observed field dependent loss. Its magnitude transpires to be rather negligible at least by comparison with the effect in $SrTiO_3$. To repeat the results of Section 4.7.3: at 151°C, 9.2 kMc/s and with a field 1.64×10^6 volts/metre the upper limit we find on the field dependent loss is 1.2×10^{-3}. This may be contrasted with an observed zero-field loss tangent of 10.45×10^{-3} under the same conditions.

In the course of planning these measurements it became obvious that the skin losses associated with electroded samples of BST-50 were only about 20 percent of the intrinsic losses under our normal experimental conditions. Their precise inportance is geometry dependent of course but their effect has been overemphasized in the past.

---

[13] B. D. Silverman, Phys. Rev. 125, 1921 (1962).

5.5 The Time Dependance of Dielectric Constant in BST-50

The drift of dielectric constant with time after the application of a dc field is described in Section 4.8 and illustrated in Fig. 21. The effect is well known and has been variously ascribed to the influence of space charge build up near the electrodes. The quantitative data presented here does not support that picture, as the following argument will show.

The effect of space charge is to reduce the field near the electrodes and increase the field in the rest of the dielectric. The magnitude of the effect depends upon the space charge density and its extent but for simplicity let us say that in effect the "electrodes" have been moved in a short way as the space charge penetrates the dielectric. The central portions of dielectric through which the microwave field propagates see an enhanced field. As the space charge creeps in the field increases and the dielectric constant of this nonlinear material drops as is qualitatively observed.

The data of Fig. 21 shows a $\Delta\epsilon/\epsilon$ of magnitude 0.017 just as a result of this time dependent drop. Denoting the original field dependent $\Delta\epsilon/\epsilon$ as η we have

$$\eta = \frac{A}{C}\,\epsilon^3(T, O)E^2$$

as given in Eq. (4).

If E changes due to creep in of the space charge we would expect a

$$d\eta = \frac{A}{C}\,\epsilon^3(T, O)\;2EdE \tag{13}$$

to result from a change in field dE applied to the central portion of the dielectric. This can be transformed to

$$d\eta = \eta \cdot \frac{2dE}{E}\,, \tag{14}$$

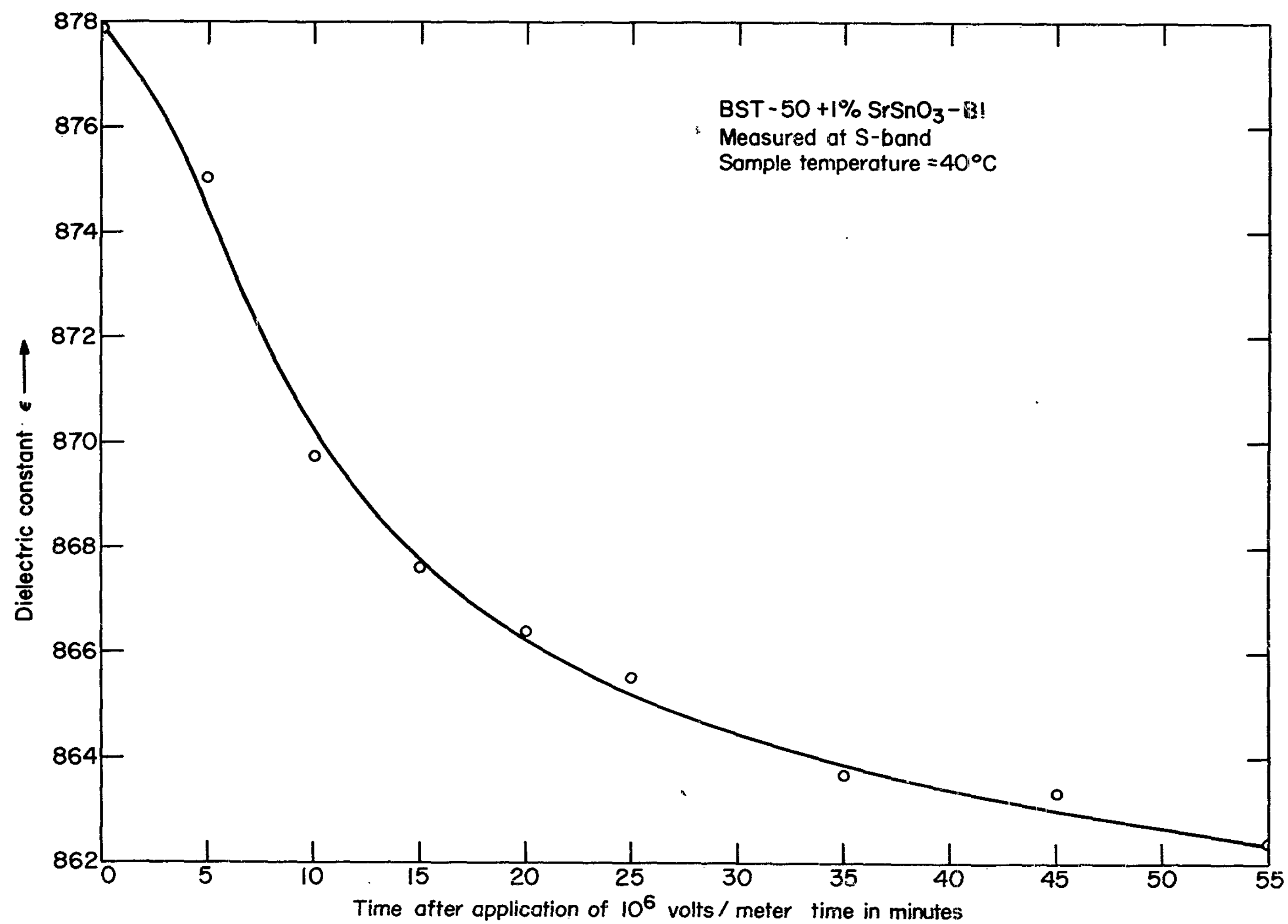

TIME DEPENDANCE OF DIELECTRIC CONSTANT WITH STEADY APPLIED FIELD

FIGURE 21

and η can be obtained from the data of Fig. 7 for this field, temperature and material (BST-50 + 1% $SrSnO_3$-B1) as 0.030. It follows that the change of field necessary to alter η by an amount 0.017 as we observe is given by

$$\frac{dE}{E} = \frac{0.017}{0.060} = 0.283 \quad . \tag{15}$$

This would imply that the space charge layer had effectively crept in a distance corresponding to 14 percent of the sample thickness at each side. The sample is $\sim$ 1000 microns in thickness and this space charge thickness is considered unreasonable when compared with the "surface layer effects" seen by other experimenters.

6. PLANS FOR THE NEXT QUARTER

The study of the effect of $SrSnO_3$ substitution in BST-50 will be continued until the characteristics of the material BST-50 + 1% $SrSnO_3$-B can be reproduced or can be ascribed to factors unconnected with the substitution.

The effect produced upon the nonlinearity of $SrTiO_3$ by various impurities will be measured in the hope that a theoretical insight to the effects will be easier to obtain in a purer crystal.

Measurements of nonlinearity in hafnate doped BST-50 materials will be conducted and impurity effects in $Cd_2Nb_2O_7$ will be studied.

Field dependent loss measurements in $SrTiO_3$ and BST-50 will be repeated and extended.

Nonlinearity measurements closer to and below the Curie temperature will be conducted if possible.

Other single crystal ferroelectric perovskites will be grown and investigated.

7. ACKNOWLEDGMENTS

Our thanks must once more be expressed to P. Balboni, D. Howe, and J. Matsinger for their care and diligence in conducting many of the measurements described herein.

8. IDENTIFICATION OF PERSONNEL

		Hours
P. B. Nutter	- Principal Research Scientist	128
R. O. Bell	- Senior Research Scientist	32
A. Paladino	- Senior Research Scientist	4
W. Bekebrede	- Senior Research Scientist	6
B. diBenedetto	- Associate Research Scientist	212
M. Harris	- Associate Research Scientist	212

Wilfred R. Bekebrede - Senior Research Scientist

Mr. Bekebrede received his A. B. degree in chemistry from Washington University in 1947. Ohio State University awarded him an M. S. in inorganic chemistry in 1952. He has completed advanced courses in chemistry, mathematics, and electronics at the Northeastern University Evening Graduate School of Engineering and at Boston University. He also attended a course in x-ray diffraction and x-ray spectroscopy techniques at the North American Phillips Company.

From 1947-1950 Mr. Bekebrede was an analytical chemist for Monsanto Chemical Company, Monsanto, Illinois. Subsequent to receiving his master's degree he did research and development work on electrolytes for the Fansteel Metallurgical Corporation, North Chicago, Illinois. In 1954, Mr. Bekebrede joined the Research Division of Raytheon Company, where he is now utilizing x-ray diffraction techniques in the study of electronic materials.

Mr. Bekebrede is a member of the American Crystallographic Association.

DISTRIBUTION LIST

Copies	
1	Airtron Division, Advanced Devices Laboratory, ATTN; Dr. J. W. Nielsen
1	Sperry Microwave Electronics Company, Clearwater, Florida ATTN: Dr. A. L. Stanford
1	General Electric Company, Defense Electronics Division, Heavy Military Electronics Department, Electronics Park, Syracuse, New York
1	General Telephone and Electronics Laboratory, Bayside Laboratories, Bayside 60, New York
1	University of Michigan, 4523 East Engineering Building, Ann Arbor, Michigan, ATTN; Prof. Howard Diamond
1	Commander, Rome Air Development Center, Air Research and Development Command, Griffiss Air Force Base, New York, ATTN: Mr. J. Schenna
1	Commander, Air Force Cambridge Research Laboratories, Bedford, Massachusetts, ATTN: Det. #2 Research Division, Mr. A. Schell
1	Sylvania Electric Products, Inc., Electronic Defense Laboratory, P. O. Box 205, Mountain View, California, ATTN: Ref: EDL 61-121
1	Motorola, Inc., Military Electronics Division, 8201 E. McDowell Road, Scottsdale, Arizona, ATTN: D. L. Fresh
1	Commanding Officer, Wright Air Development Division, Air Research and Development Command, Wright Patterson Air Force Base, Ohio, ATTN: Mr. Carl Greene, Materials Control
1	Commanding Officer, U. S. Army Signal Research and Development Laboratory, Fort Monmouth, New Jersey, ATTN: SELRA/PRM (Mr. I. Reingold)
1	Columbia University, Department of Electric Engineering, New York 27, New York, ATTN: Mr. Victor Granatstein
1	General Telephone and Electronics, Microwave Physics Laboratory, Palo Alto, California
2	Commanding Officer U. S. Army Electronics Research and Development Laboratory Fort Monmouth, New Jersey, ATTN: SELRA/PRG (Mrs. Green), ATTN: SELRA/PEM (Mr. J. Agrios)
1	Rutgers, The State University, Department of Electric Engineering, New Brunswick, New Jersey, ATTN: Mr. Robert G. Pecina
1	Electronic Communications, Inc., Research Division, 1830 York Road, Timonium, Maryland

DISTRIBUTION LIST (Cont'd)

Copies	
1	Bureau of Ships - 691 B-2C, Electronics Division, Room 3329, Main Navy Building, Washington 25, D. C., ATTN: Leo V. Gumina
1	Commander, Rome Air Development Center, Air Research and Development Command, Griffiss Air Force Base, New York, ATTN: Mr. Patsy A. Romanelli - RCLRA-2
1	Commander, Hq., Detachment 2, AFRD, L. G. Hanscom Field, Bedford, Massachusetts, ATTN: Mr. Charles E. Ellis, Jr., CRRDM
1	Radio Corporation of America, Somerville, New Jersey, ATTN: Dr. B. Schwartz
1	Texas Instruments Incorporated, Apparatus Division, Research and Development Department, P. O. Box 5012, Dallas 22, Texas
1	Commanding Officer, Aeronautical Systems Division, Wright-Patterson Air Force Base, Ohio, ATTN: C. Wittebort, ASRCPT
1	Clevite Corporation, Electronic Research Division, 540 East 105th Street, Cleveland 8, Ohio, ATTN: Mr. B. Jaffee
1	Airborne Instruments Laboratory, Division of Cutler-Hammer, Deer Park, New York, ATTN: Mr. Larry Wright
1	National Bureau of Standards, Engineering Electronics Section, Washington 25, D. C., ATTN: Mr. Gustave Shapiro, Chief
6	Commanding Officer, U. S. Army Electronics Research and Development Laboratory, Fort Monmouth, New Jersey, ATTN: SELRA/PEM (Mr. J. Charlton)
1	OASD (R&E), Room 3E1065, The Pentagon, Washington 25, D. C. ATTN: Technical Library
1	Chief of Research and Development, OCS, Department of the Army, Washington 25, D. C.
1	Commanding General, U. S. Army Materiel Command, Washington 25, D. C., ATTN: R&D Directorate
1	Commanding General, U. S. Army Electronics Command, Fort Monmouth, New Jersey, ATTN: AMSEL-AD
1	Director, U. S. Naval Research Laboratory Washington 25, D. C., ATTN: Code 2027
1	Commander, Aeronautical Systems Division, Wright-Patterson Air Force Base, Ohio, ATTN: ASAPRL
1	Hq., Electronic Systems Division, L. G. Hanscom Field, Bedford, Massachusetts, ATTN: ESAL

DISTRIBUTION LIST (Cont'd)

Copies	
1	Commander, Air Force Cambridge Research Laboratories, L. G. Hanscom Field, Bedford, Massachusetts, ATTN: CRO
1	Commander, Air Force Command and Control Development Division, L. G. Hanscom Field, Bedford, Massachusetts, ATTN: CRZC
1	Commander, Rome Air Development Center, Griffiss Air Force Base, New York, ATTN: RAALD
1	USAELRDL Liaison Office Rome Air Development Center ATTN: RAOL Griffiss Air Force Base, New York
10	Commander, Armed Services Technical Information Agency, Arlington Hall Station, Arlington 12, Virginia, ATTN: TISIA
2	Chief, U. S. Army Security Agency, Arlington Hall Station, Arlington 12, Virginia
1	Deputy President, U. S. Army Security Agency Board, Arlington Hall Station, Arlington 12, Virginia
1	Commanding Officer, Harry Diamond Laboratories, Washington 25, D. C. ATTN: Library, Room 211, Building 92
1	Corps of Engineers Liaison Office, U. S. Army Electronics Research and Development Laboratory, Fort Monmouth, New Jersey
1	AFSC Scientific/Technical Liaison Office, U. S. Naval Air Development Center, Johnsville, Pennsylvania
1	AFSC Liaison Office, Naval Air R&D Activities Command, Naval Air R&D Activities Command, Johnsville, Pennsylvania
1	Commanding Officer, U. S. Army Electronics Materiel Support Agency, Fort Monmouth, New Jersey, ATTN: SELMS-ADJ
1	Marine Corps Liaison Office, U. S. Army Electronics Research and Development Laboratory, Fort Monmouth, New Jersey, ATTN: SELRA/LNR
1	Commanding Officer, U. S. Army Electronics Research and Development Laboratory, Fort Monmouth, New Jersey, ATTN: Director of Research or Engineering
1	Commanding Officer, U. S. Army Electronics Research and Development Laboratory, Fort Monmouth, New Jersey, ATTN: Technical Documents Center
1	Commanding Officer, U. S. Army Electronics Research and Development Laboratory, Fort Monmouth, New Jersey, ATTN; SELRA/ADJ (FU #1)

DISTRIBUTION LIST (Cont'd)

Copies

1 Commanding Officer, U. S. A. Electronics Research and Development, Fort Monmouth, New Jersey
ATTN: SELRA/PE (Dr. E. Both)
ATTN: SELRA/PE (Division Director)

2 Advisory Group on Electron, 346 Broadway, New York 13, New York

3 Commanding Officer, U. S. Army Electronics Research and Development Laboratory, Fort Monmouth, New Jersey, ATTN: SELRA/TNR (FOR RETRANSMITTAL TO ACCREDITED BRITISH AND CANADIAN GOVERNMENT REPRESENTATIVES)

1 Commanding General, U. S. Army Combat Developments Command, Fort Belvoir, Virginia, ATTN: CDCMR-E

1 Commanding Officer, U. S. Army Combat Developments Command, Communications-Electronics Agency, Fort Huachuca, Arizona

1 Director, Fort Monmouth Office, U. S. Army Combat Developments Command, Communications-Electronics Agency, Building 410, Fort Monmouth, New Jersey

1 AFSC Scientific/Technical Liaison Office, U. S. Army Electronics Research and Development Laboratory, Fort Monmouth, New Jersey

1 Commanding Officer and Director, U. S. Navy Electronics Laboratory, San Diego 52, California

AD Div. 25/2 UNCLASSIFIED

Raytheon Company, Research Division, Waltham, Mass.
MICROWAVE FERROELECTRICS
Report No. 10 Progress 16 December 1962 - 15 March 1963
by P.B. Nutter, M. Harris, and B. di Benedetto. 51 p. illus. and Tables
(Report S-532)
Contract DA 36-039-sc-89126 Unclassified

DESCRIPTORS: Material Investigation, Dielectric Constant, Loss Tangent, Nonlinearity data.

Indentifiers: Single crystal $KTaO_3$, Polycrystalline $PbTiO_3$.

Several batches of $Ba_{0.5}Sr_{0.5}TiO_3$ + 1% SrSnO3 ceramic have been prepared and those which have been measured all exhibit a slightly larger nonlinearity than pure $Ba_{0.5}Sr_{0.5}TiO_3$ material. One sample only shows a markedly larger nonlinearity which has been confirmed by repeated measurements and by using different measuring techniques. The reason for its superiority over supposedly identical materials has not been established. Losses in other doped materials have been measured. The field dependent loss in $Ba_{0.5}Sr_{0.5}TiO_3$ material has been measured and an upper limit

AD Div. 25/2 UNCLASSIFIED

Raytheon Company, Research Division, Waltham, Mass.
MICROWAVE FERROELECTRICS
Report No. 10 Progress 16 December 1962 - 15 March 1963
by P.B. Nutter, M. Harris, and B. di Benedetto. 51 p. illus. and Tables
(Report S-532)
Contract DA 36-039-sc-89126 Unclassified

DESCRIPTORS: Material Investigation, Dielectric Constant, Loss Tangent, Nonlinearity data.

Indentifiers: Single crystal $KTaO_3$, Polycrystalline $PbTiO_3$.

Several batches of $Ba_{0.5}Sr_{0.5}TiO_3$ + 1% SrSnO3 ceramic have been prepared and those which have been measured all exhibit a slightly larger nonlinearity than pure $Ba_{0.5}Sr_{0.5}TiO_3$ material. One sample only shows a markedly larger nonlinearity which has been confirmed by repeated measurements and by using different measuring techniques. The reason for its superiority over supposedly identical materials has not been established. Losses in other doped materials have been measured. The field dependent loss in $Ba_{0.5}Sr_{0.5}TiO_3$ material has been measured and an upper limit

AD Div. 25/2 UNCLASSIFIED

Raytheon Company, Research Division, Waltham, Mass.
MICROWAVE FERROELECTRICS
Report No. 10 Progress 16 December 1962 - 15 March 1963
by P.B. Nutter, M. Harris, and B. di Benedetto. 51 p. illus. and Tables
(Report S-532)
Contract DA 36-039-sc-89126 Unclassified

DESCRIPTORS: Material Investigation, Dielectric Constant, Loss Tangent, Nonlinearity data.

Indentifiers: Single crystal $KTaO_3$, Polycrystalline $PbTiO_3$.

Several batches of $Ba_{0.5}Sr_{0.5}TiO_3$ + 1% SrSnO3 ceramic have been prepared and those which have been measured all exhibit a slightly larger nonlinearity than pure $Ba_{0.5}Sr_{0.5}TiO_3$ material. One sample only shows a markedly larger nonlinearity which has been confirmed by repeated measurements and by using different measuring techniques. The reason for its superiority over supposedly identical materials has not been established. Losses in other doped materials have been measured. The field dependent loss in $Ba_{0.5}Sr_{0.5}TiO_3$ material has been measured and an upper limit

AD Div. 25/2 UNCLASSIFIED

Raytheon Company, Research Division, Waltham, Mass.
MICROWAVE FERROELECTRICS
Report No. 10 Progress 16 December 1962 - 15 March 1963
by P.B. Nutter, M. Harris, and B. di Benedetto. 51 p. illus. and Tables
(Report S-532)
Contract DA 36-039-sc-89126 Unclassified

DESCRIPTORS: Material Investigation, Dielectric Constant, Loss Tangent, Nonlinearity data.

Indentifiers: Single crystal $KTaO_3$, Polycrystalline $PbTiO_3$.

Several batches of $Ba_{0.5}Sr_{0.5}TiO_3$ + 1% SrSnO3 ceramic have been prepared and those which have been measured all exhibit a slightly larger nonlinearity than pure $Ba_{0.5}Sr_{0.5}TiO_3$ material. One sample only shows a markedly larger nonlinearity which has been confirmed by repeated measurements and by using different measuring techniques. The reason for its superiority over supposedly identical materials has not been established. Losses in other doped materials have been measured. The field dependent loss in $Ba_{0.5}Sr_{0.5}TiO_3$ material has been measured and an upper limit

set upon its value. The value of the field dependent loss is small compared with the intrinsic zero-field loss at X-band, at 150°C and for fields of 1.6×10^6 volts/meter.

set upon its value. The value of the field dependent loss is small compared with the intrinsic zero-field loss at X-band, at 150°C and for fields of 1.6×10^6 volts/meter.

set upon its value. The value of the field dependent loss is small compared with the intrinsic zero-field loss at X-band, at 150°C and for fields of 1.6×10^6 volts/meter.

set upon its value. The value of the field dependent loss is small compared with the intrinsic zero-field loss at X-band, at 150°C and for fields of 1.6×10^6 volts/meter.